Modeling on Fluid Flow and Inclusion Motion in Centrifugal Continuous Casting Strands

Qiangqiang Wang [1], Lifeng Zhang[1], Seetharaman Sridhar[2]

[1]School of Metallurgical and Ecological Engineering
University of Science and Technology Beijing
Beijing 100083, China
[2]Warwick Manufacturing Group, University of Warwick
Coventry, CV4 7AL, UK
Correspondent：Lifeng Zhang; tel.: +86-10-62332267; fax: +86-10-62332267; E-mail: zhanglifeng@ustb.edu.cn; postal address: School of Metallurgical and Ecological Engineering, University of Science and Technology Beijing, No. 30, Xueyuan Road, Haidian District, Beijing 100083, China

Abstract

In the current study, a three-dimensional multi-phase turbulent model was established to study the transport phenomena during centrifugal continuous casting process. The effects of nozzle position, casting speed and rotation speed on the flow pattern, centrifugal force acting on the molten steel, level fluctuation, gas entrainment, shear stress on mold wall and motion of inclusions during centrifugal continuous casting process were investigated. Volume of Fluid model was used to simulate the molten steel-air two-phase. The level fluctuation and the gas entrainment during casting were calculated by user-developed subroutines. The trajectory of inclusions in the rotating system was calculated using the Lagrangian approach. The results show that during centrifugal continuous casting, a large amount of gas was entrained into the molten steel, and broken into bubbles of various sizes. The greater the distance to the mold wall, the smaller the centrifugal force. And the rotation speed had the most important influence on the centrifugal force distribution at the side region. Angular moving angle of the nozzle with 8° and keeping the rotation speed with 60 revolutions per minute can somehow stabilize the level fluctuation. The increase of angular angle of nozzle from 8° to 18° and rotation speed from 40 to 80 revolutions per minute favored to decrease the total volume of entrained bubbles, while the increase of distance of nozzle moving left and casting speed had reverse effects. The trajectories of inclusions in the mold were irregular, and then rotated along the strand length. After penetrating a certain distance, the inclusions gradually moved to the center of billet and gathered there. To discuss the heat transfer, solidification and inclusions entrapment during centrifugal continuous casting, more work will be performed.

Key words：

Centrifugal continuous casting, Fluid flow, Gas entrainment, Inclusion motion

I. INTRODUCTION

Centrifugal continuous casting (CCC) is an industrial steel casting process during which molten steel is injected into a round mold. During the pouring stage, the entire system is rotated along its axis at a certain rotational speed. The molten steel flows down into the mold through a no-straight nozzle, and once touching the side wall of mold, the molten steel rotates and moves towards the inner surface of the copper mold due to the centrifugal force stemming from the spinning mold. The solidifying shell grows as the steel is continuously withdrawn from the bottom of the mold. In the secondary cooling region, the back-up rolls around the round billet also spin in order to rotate the billet at the same rotation speed to that of the copper mold.

There are very few reported studies on steel centrifugal continuous casting. However, the centrifugal ingot or pipe casing technology using horizontal or vertical devices has been developed for several decades and applied for the production of steel pipes [1-4]. In 1957, the horizontal centrifugal casting was used to produce 50 mm pipes [1]. Due to the fact that the technique has not yet been optimized in the early days, the rejection ratio of cast pipes at several plants all exceeded permissible standards. In 1958, pipes with 200-600 mm diameter were cast by centrifugal casting which had both vertical and horizontal forms [2]. It was reported that the wear resistance of a high-strength cast iron with centrifugal casting averaged 220% higher than that by stationary ingot casting[3]. Characteristics of the centrifugal casting include:

- Relatively less defects than traditional stationary casting;
- More non-metallic inclusions toward the bore so that they can be machined off;
- Better mechanical properties;
- Higher production rate;
- Possible to be used to functionally fabricate gradient metal matrix composite materials.

The concept of producing castings in a rotating mold under a continuous operation can

date back to 1904 and can be found in several patents [5-7]. It was designed to cast pipes. During pouring, the finished casted pipes were pulled out without stopping the rotation of the mold. For CCC system, the fluid flow plays an important role as the high-speed discharging flow has a great influence on gas entrainment, motion of inclusions [8, 9], shell formation and the lifetime of copper mold. It is difficult to watch or measure the fluid flow velocity and multiphase phenomena in continuous casting strands because of the opaque nature of the melt and the mold. Therefore, in order to understand the steel CCC process of round billets, mathematical modeling of the fluid flow phenomena is a feasible choice. Many turbulent models and multiphase models have been used for the fluid flow in gas-stirred steel refining processes [10-12] and steel continuous casting processes [13-23], as summarized in Table I. However, so far very few investigations on CCC process were reported.

Table I. Reported studies on the fluid flow phenomenon during steel continuous casting process

Authors	Multiphase Model	Turbulent model	Main Findings	Year	Ref
Lait	NA	One-dimensional finite-difference model	- Calculation of the temperature field and pool profiles of continuous casting slab of stainless steel and low-carbon billet.	1974	[13]
Hirt	Volume of fluid (VOF)	NA	- VOF method for treating complicated free boundary configurations.	1981	[14]
Thomas	Eulerian-Eulerian model	Standard k-ε	- Effect of argon bubbles on the flow pattern in continuous casting mold.	1994	[15]
Ho	SOLA method	Standard k-ε	- Simultaneous consideration of SEN design, the number and the size of outlets.	1996	[16]
Panaras	finite volume methodology(FVM)	Standard k-ε	- Revealing a predominant length and frequency free surface wave; - Association of wave instability with emulsification and a critical casting speed.	1998	[17]
Tan	SOLA-VOF	Standard k-ε	- Influence of the size and the position of the circumfluence region in the mold on the surface oscillation morphology.	2003	[18]
Zhang	NA	Standard k-ε	- Asymmetrical temperature distribution in the mold generated by one-side clogging SEN.	2008	[19]
Thomas	NA	Standard k-ε	- More susceptible to problems from asymmetric flow and excessive surface velocities by a mountain-shaped bottom SEN	2008	[20]

			than well-shaped bottom SEN.		
Zhang	VOF	Standard k-ε	- Simulation of cast start using dynamic mesh; - Investigation of casting speed change, temperature fluctuation and steel grade mixing.	2010	[21, 22]
Ismael	VOF	Standard k-ε	- Effect of deviation of the nozzle towards the inner mold radius on the symmetrical flow pattern and better meniscus control.	2013	[23]

The multiphase model of VOF is an eulerian method that uses a volume fraction to determine the location of the interfaces of different phases in all cells of a computational domain, and it has been widely used to track free surface [14, 23-27]. Hugo [28] employed RSM turbulence model and VOF multiphase model to study the effect of the internal SEN design on the flow pattern in a funnel thin slab caster and concluded that the jets oscillation had its origin from the inside of the SEN. Mirandal [25] chose k-ε turbulence model and VOF model to study the flow pattern prevailing at the steel-slag interface in a water model of a slab continuous casting mold, and obtained a good agreement between simulated and experimented data. Wang and Zhang [21] employed this algorithm to simulate the interface evolution between the molten steel and air during cast start of steel continuous casting process. Tan [18] used this method to simulate the shape of free surface in a continuous casting mold and analyzed the mechanism of the surface oscillation. During steel continuous casting process, the entrainment of non-metallic inclusions is also an important phenomenon. Poor control of flow can cause inclusions to be captured in the final steel product [29]. Due to their low volume fraction of inclusions in molten steel, the trajectory of inclusions was often calculated by Lagrangian approach [30-33].

In the current study, the multiphase fluid flow and motion of inclusions during steel CCC process were studied. The effects of nozzle position, rotation speed of the mold and casting speed on the transport phenomena were discussed. To fully study the complicated phenomena during steel CCC process, the current article focused on the turbulent flow as the first part of systematic scientific studies, followed by the detection

of non-metallic inclusion during industrial trials of CCC process and the model of heat transfer and solidification and the prediction of final locations of inclusions in the billet, which are reported in another two papers by the current authors [34, 35].

II. MATHEMATICAL FORMULATION

A. *CCC Process and Mesh Used in the Simulation*

Figure 1 shows the schematic of CCC process. Unlike the conventional submerged entry nozzle (SEN), the nozzle used for CCC process has a curved shape and 22 mm circular outlet, and is placed above the mold. This arrangement of the outlet does not directly face the meniscus but contributes to the rotation of jet flow entering the mold instead. During casting, the atmosphere between mold and tundish is shrouded by an inert gas in order to avoid re-oxidation. A special oil is also added to the top surface of the mold to provide thermal and chemical insulation for the steel. The liquid oil is entrained into the gap between the shell and mold by the downward motion of the steel shell, where it encourages a uniform heat transfer and helps to lubricate and prevent sticking of the solidifying shell to the mold.
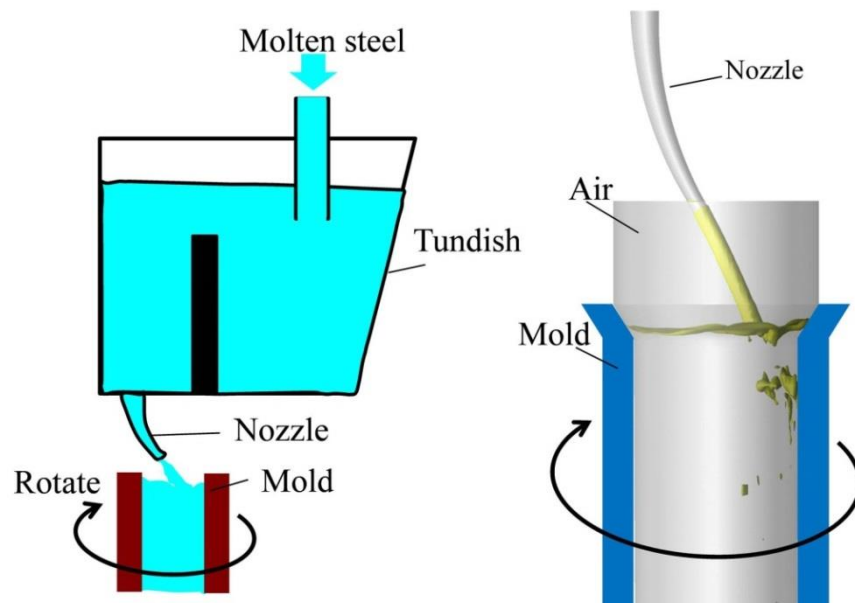

Fig.1 Schematic of CCC process with round-type mold

Structured grids were employed for the mesh system of mold and nozzle, as shown in Figure 2. The height of domain in the current simulation was 16 m including the nozzle, air region, mold and secondary cooling sections. The total number of grid was 700,000. As VOF method requires a fine mesh to achieve the accuracy for free surface movement that is needed for predicting level fluctuations [36], in the current study, to save computation time and obtain level fluctuation, the spacing of adjacent meshes was set to increase gradually along the casting direction.
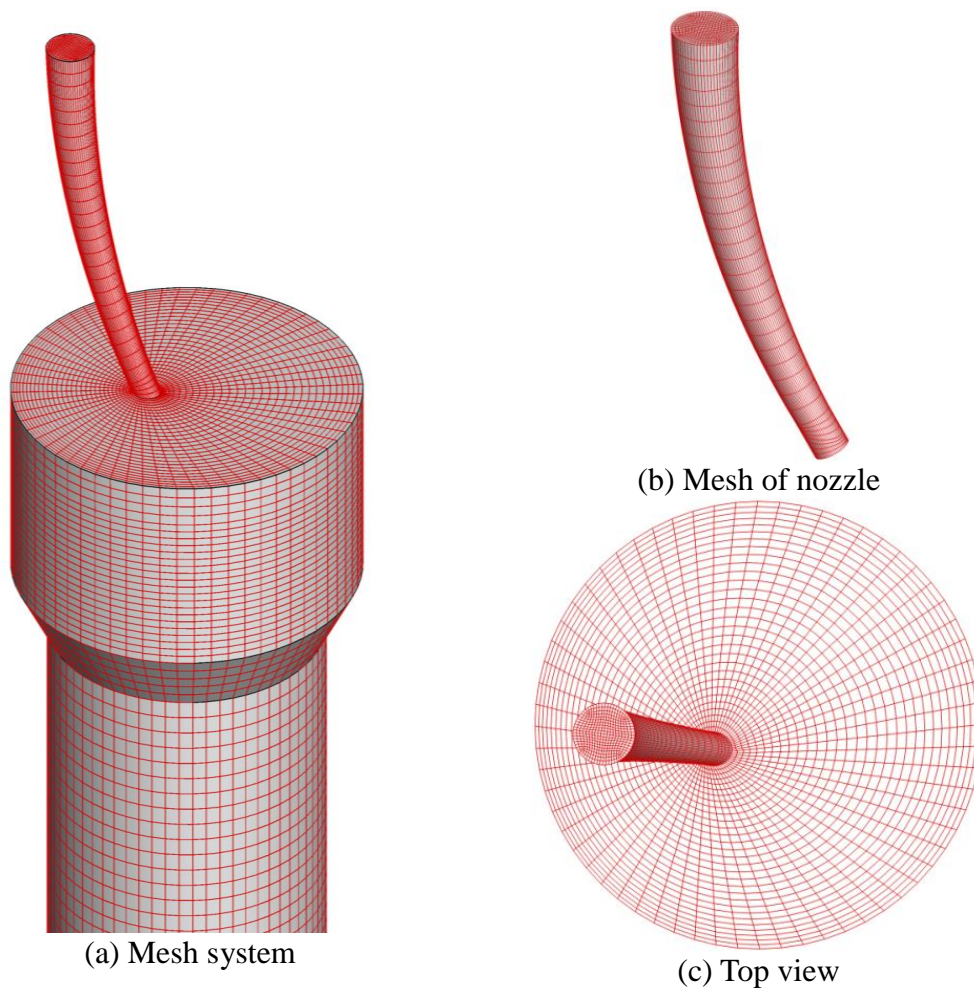

(a) Mesh system

(b) Mesh of nozzle

(c) Top view

Fig.2 Mesh system for the computational domain

In addition, four planes at 1 m, 6 m, 11 m and 15 m below meniscus were picked up to investigate the location of inclusions on the cross sections, as given in Figure 3.
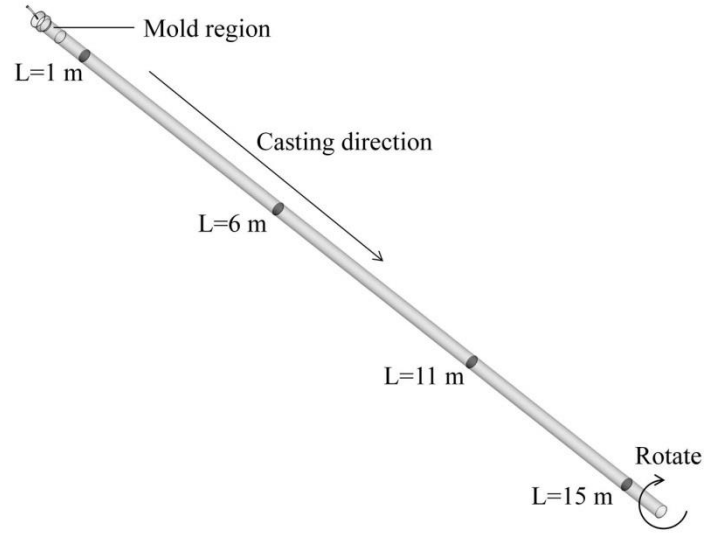
Fig.3 Cross sections to show locations of inclusions

B. *Governing Equations*

For the VOF model [14], a single set of momentum equations is shared by two fluids, the molten steel and the air phase in the current study. The volume fraction of the fluids is tracked throughout the domain. The tracking of the interface is accomplished by the solution of a continuity equation for the volume fraction of both phases:

$$\frac{\partial \alpha_q}{\partial t} + u_j \frac{\partial \alpha_q}{\partial x_i} = 0 \tag{1}$$

where α_q is the volume fraction of phase "q" (%). A single momentum equation is solved throughout the domain as follows:

$$\frac{\partial (\rho u_j)}{\partial t} + \frac{\partial (\rho u_i u_j)}{\partial x_i} = -\frac{\partial P}{\partial x_j} + \frac{\partial}{\partial x_i}\left(\mu_{eff} \left(\frac{\partial u_i}{\partial x_j} + \frac{\partial u_j}{\partial x_i} \right) \right) \tag{2}$$

where μ_{eff} is the effective dynamic viscosity of the continuous phase (Pa·s). The resulting field is shared among the phases. Thus, the momentum-transfer equation is

dependent on the volume fraction of the two-phase flow through the averaged properties of density and viscosity of the mixture that are given by:

$$\rho = \alpha_l \rho_l + \alpha_g \rho_g \tag{3}$$

$$\mu = \alpha_l \mu_l + \alpha_g \mu_g \tag{4}$$

where ρ is the mixed phase density (kg/m^3), μ is the mixed phase viscosity (Pa·s), α_l and α_g are volume fraction of the molten steel and air phase (%). A constraint of the system implies that the sum of the volume fractions of both phases in the shared cells should be equal to 1, namely:

$$\alpha_l + \alpha_g = 1 \tag{5}$$

In the current study, the standard k-ε turbulence model was chosen for the liquid phase, which requires the solution of two additional transport equations to find the turbulent kinetic energy, k, and the turbulent dissipation rate, ε.

$$\frac{\partial(\rho k)}{\partial t} + \frac{\partial}{\partial x_i}\left(\rho u_i k - \frac{\mu_{eff}}{\sigma_k}\frac{\partial k}{\partial x_i}\right) = \mu \frac{\partial u_j}{\partial x_i}\left(\frac{\partial u_i}{\partial x_j} + \frac{\partial u_j}{\partial x_i}\right) - \rho\varepsilon \tag{6}$$

$$\frac{\partial(\rho\varepsilon)}{\partial t} + \frac{\partial}{\partial x_i}\left(\rho u_i \varepsilon - \frac{\mu_{eff}}{\sigma_\varepsilon}\frac{\partial\varepsilon}{\partial x_i}\right) = C_1 \mu_t \frac{\varepsilon}{k}\frac{\partial u_j}{\partial x_i}\left(\frac{\partial u_i}{\partial x_j} + \frac{\partial u_j}{\partial x_i}\right) - C_2 \frac{\varepsilon}{k}\rho\varepsilon \tag{7}$$

The turbulent viscosity is given by[37, 38]:

$$\mu_t = \rho C_\mu \frac{k^2}{\varepsilon} \tag{8}$$

C_1, C_2, C_μ, σ_k and σ_ε are empirical constants, respectively, and reported in literatures [16, 39-41]. The combination of VOF model and standard k-ε model to predict the interface of two phases and the flow field in continuous casting mold has been validated with water model by current author, and indicated a well agreement between the measurement and the calculation [21].

The trajectories of inclusions were calculated using Lagrangian approach which treats inclusion particles as a discrete phase [42], by considering the force balance acting on them [43].

$$\frac{du_{pi}}{dt} = \frac{18\mu}{\rho_P d_P^2} \frac{C_D \operatorname{Re}_P}{24}\left(u_i - u_{pi}\right) + \frac{\rho_P - \rho}{\rho} g_i + \frac{1}{2}\frac{\rho}{\rho_P}\frac{d}{d_t}\left(u_i - u_{pi}\right) + \frac{\rho}{\rho_P}u_i\frac{\partial u_i}{\partial x_i} + F_C \quad (9)$$

where u_{Pi} is particle velocity at direction i (m/s), t is time (s), C_D is a dimensionless drag coefficient, Re_P is a particle Reynolds number, d_P is particle diameter (m), ρ_P is inclusion density (kg/m^3). The first term here is the drag force per unit of particle mass, the second term is gravitational force, the third term is the virtual mass force accelerating the fluid surrounding the particle, and the fourth term is the force stemming from the pressure gradient in the fluid. To incorporate the centrifugal force (F_C) acting on particles due to the rotation of mold, a user defined subroutine was developed. Since the current study ignored the interaction between the advancing solidified steel and the non-metallic inclusion particles, the capillary force was not considered. To incorporate the "stochastic" effect of turbulent fluctuations on the motion of inclusions, the "random walk" model was used [44], in which the fluid flow velocity was the sum of the local mean fluid velocity and the random fluctuation velocity. The random fluctuation velocity was based on a Gaussian-distributed random number chosen according to the local turbulence kinetic energy. The variation of random number produced a new instantaneous fluctuation velocity at a frequency equal to the characteristic lifetime of the eddy. In the current study, only the effect of fluid flow on the motion of inclusions

was investigated. To further study the motion and entrapment of inclusions during CCC process, the effects of heat transfer and solidification will be discussed in another study [35].

C. *Boundary Conditions*

A constant velocity was imposed as the nozzle inlet condition. The velocity was calculated according to the casting speed, the billet size and the cross area of the inlet. A pressure outlet condition as zero pascal gauge pressure was used on the top surface of air region. At the domain exit, 15.89 m below the meniscus, the fixed velocity was employed, corresponding to the casting speed. The rotation of the centrifugal system was achieved through the wall rotation of the mold and the secondary cooling zone, *i.e.*, the wall of mold and secondary cooling zone were set as moving wall with a fixed rotation speed and a no-slip shear condition. The surface tension effect between the air and molten steel was taken into account using CSF (Continuous Surface Force) model [45, 46], which interpreted the surface tension as a continuous, three-dimensional effect across an interface, rather than as a boundary value condition on the interface. The discretized equations were solved for velocity and pressure by the Pressure-Implicit with Splitting of Operators scheme [47] which is highly recommended for all transient flow calculation. Due to the difficulty in convergence and time-consuming of the two-phase modeling, the non-iterative time-advancement (NITA) scheme was employed which preserved overall temporal accuracy. The NITA scheme does not need the outer iterations, performing only a single outer iteration per time-step, which significantly speeds up the transient simulation. For the current simulations, the time step was set to 0.0001 seconds at the start and was increased to 0.001 seconds after the fluid flow was fully developed after twenty seconds.

D. *Parameters*

During the current CCC process, no flux is used at the mold, instead, liquid oil poured during CCC to lubricate the shell and mold copper plate. Nitrogen gas is pursed on the

top surface of the mold to isolate air from the molten steel. Since the molten steel at the meniscus touches the gas with low temperature, small pieces of frozen shell are formed on the meniscus and the frozen shell combine with the lining materials from the nozzle at sometimes, as shown in Figure 4. These shell needs to be manually taken away with a steel rod. Improper arrangement of nozzle may wash severely the solidifying front, high casting speed and rotation speed can result in violent level fluctuation, serious gas entrainment and entrainment of the frozen shell pieces mentioned above.

(a) Frozen shell   (b) Location A
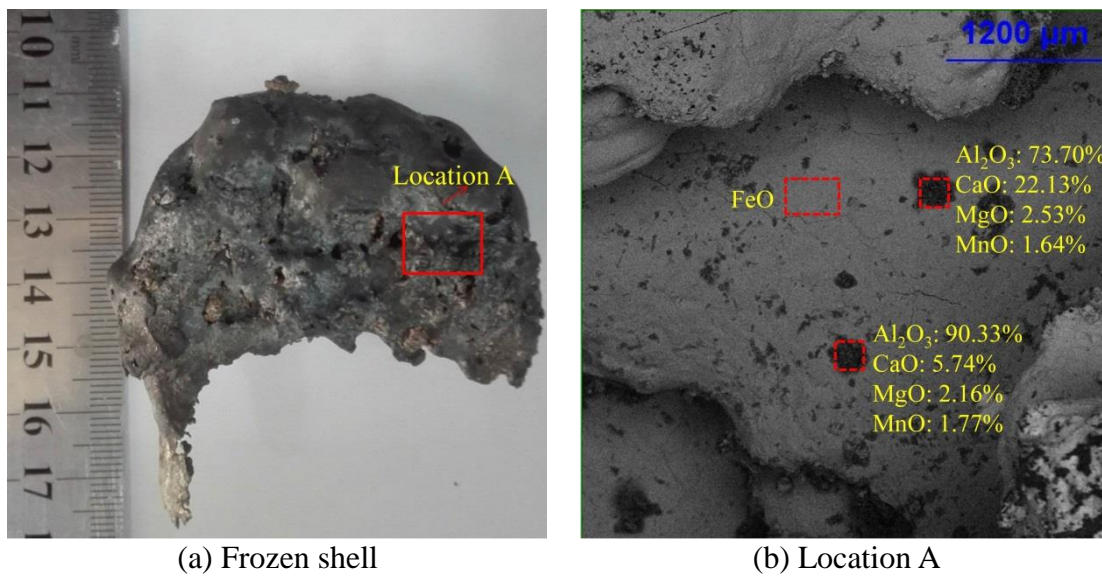
Fig.4 Schematic of frozen shell and compositions on the surface of location A

Hence, in the current study, the effects of nozzle position, casting speed and rotation speed were investigated to study the relevant transport phenomena, such as flow pattern, centrifugal force, level fluctuation, gas entrainment, shear stress on mold wall and motion of inclusions. For the nozzle position, three horizontal moving positions l (horizontal distance from the center of round mold to the center of the nozzle inlet), 100 mm to left, 110 mm to left and 120 mm to left, and three clockwise angular moving positions of the nozzle θ, $i.e.$, 8°, 13° and 18°, were investigated, as shown in Figure 5. The casting speeds (V_c) were 1.27 m/min, 1.905 m/min and 2.54 m/min, respectively. The rotation speeds (n) were 40 revolutions per minute (rpm), 60 rpm and 80 rpm, respectively.

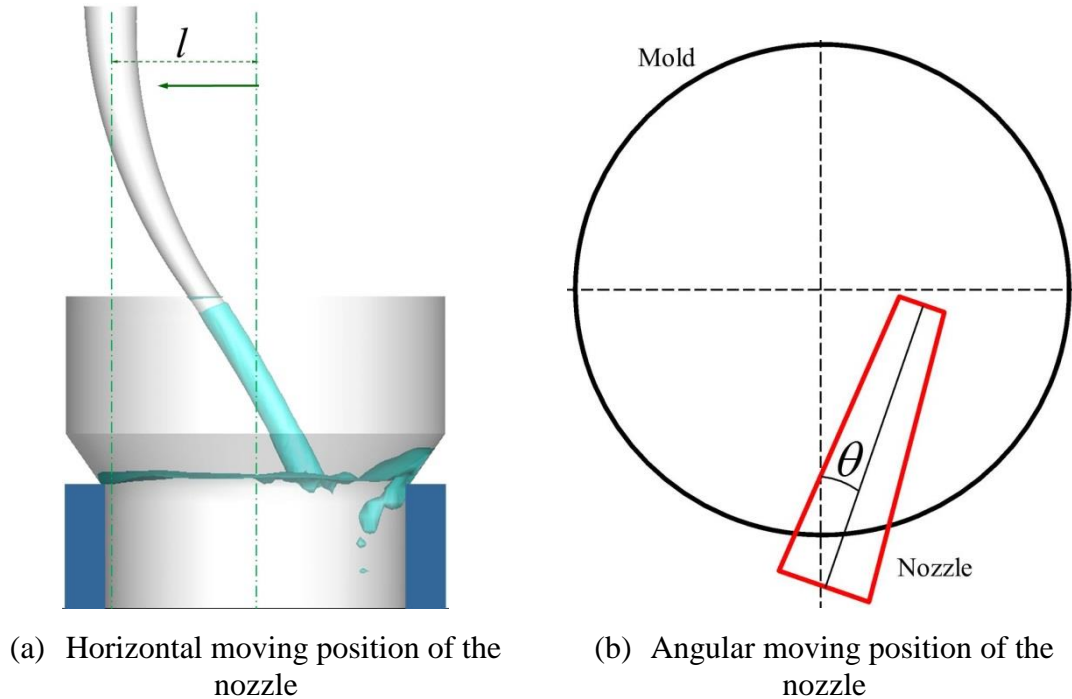|	
(a) Horizontal moving position of the nozzle	(b) Angular moving position of the nozzle

Fig.5 Study on the position of nozzle

Physical property parameters used for the current simulation are listed Table II. Inclusions were assumed to be spherical with constant diameters and collision, growth and break up of inclusions were neglected. A constant density of 5,000kg/m^3 for inclusions was assumed [48]. To obtain significant statistics, five thousand inclusions with the same size were injected into the mold at each time step through the inlet of nozzle after the calculation of fluid flow reached steady state, and the effect of inclusions on fluid flow was ignored. Particles were assumed to escape from the domain exit and reflected at the wall of mold and secondary cooling zone. The entrapment of inclusions to the solidified shell will be reported in another paper submitted by the current author. The spatial coordinates of inclusions were exported once inclusions passed through the four cross sections described in Fig.3. In the current work, the presence of oil added to the top surface was ignored and air was assumed above the molten steel.

Table II. Dimensions and parameters

Parameter	Value	Parameter	Value
SEN port diameter	22 mm	Velocity at inlet (V_c=1.27 m/min)	0.6998 m/s
Mold working length	430 mm	Turbulent kinetic energy at inlet	0.001 m²/s²
Mold radius	115 mm	Turbulent dissipation rate at inlet	0.005 m²/s³
Initial height of air above the molten steel	195 mm	Density of liquid steel	7020 kg/m³
Domain length	16 m	Viscosity of liquid steel	0.0067 kg/(m·s)
Mold rotational speed, n	40-80 rpm	Density of air	1.225 kg/m³
Horizontal moving distance of nozzle, l	100-120 mm	Viscosity of air	1.7894e⁻⁵ kg/(m·s)
Angular moving angle of nozzle, θ	8-18°	Gravity acceleration rate	9.81 m/s²
Casting speed, V_c	1.27-2.54 m/min	Surface tension of molten steel	1.85 N/m

E. *User Developed Subroutines*

To achieve quantitative results of gas entrainment and level fluctuation of the free surface under different casting conditions, several user developed subroutines, simplified as UDFs, were developed, combining the calculation using the commercial software Fluent [47]. Models and UDFs used in this simulation are shown in Figure 6.
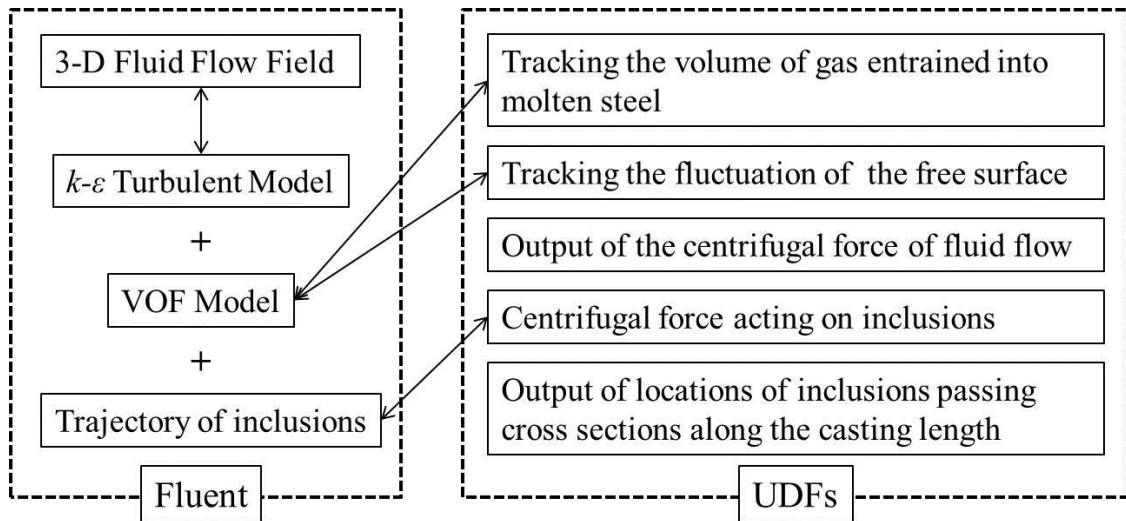

Fig.6 Schematic of models and UDFs used in the current study

The volume of gas below the top surface of molten steel was regarded as the gas entrainment, calculated by the following equation:

$$V_g = f_{g,l} \cdot V_{cell} \tag{10}$$

where V_g is the volume of gas entrained into the bulk (m³), $f_{g,l}$ is the volume fraction of gas entrained (%) and V_{cell} is the volume of cell where air-phase stays (m³).

In order to track the fluctuation of the free surface, 1000 balls were uniformly placed on the top surface of the molten steel. The particle is 2 mm diameter and 200 kg/m³ density. The density was determined considering the value was far larger than that of air phase (1.225 kg/m³) and far smaller than that of liquid steel (7020 kg/m³). So that particles always stayed at the meniscus or nearby. In addition, a user subroutine was developed to prevent the horizontal motion of inclusions, and only vertical motion of inclusions was allowed. At each time step, the locations of these balls were saved and exported to a file. The level profile was then achieved by post-processing the locations of balls with time by subtracting the original vertical coordinate of the free surface.

To evaluate the centrifugal effect under different casting conditions, the centrifugal force along the diameter at the cross section 15 m below the free surface was calculated. The centrifugal forces are created by the circumferential motion. The linear velocity of a point on a rotating rigid object at a distance from the axis of rotation represents the tangential velocity of that point. For the rotation around a fixed point, the path of any point on a revolving body is a circle, and its linear velocity at any moment is always tangent to that circle. Therefore, the centrifugal force per unit volume can be defined as follow:

$$F_C = \frac{\rho v^2}{r} \tag{11}$$

where F_C is the centrifugal force per unit volume (N/m³); ρ is the density of the mixture (kg/m³); v is the tangential velocity (m/s); and r is the radius from center to the point (m).

III. MULTIPHASE FLUID FLOW DURING CCC

A. *Flow Pattern*

Figure 7-9 show the three dimensional interface (0.5 iso-surface of gas fraction) between the molten steel and air phase, the velocity vector, k and ε at the interface under different conditions, respectively. To show the velocity vector more clearly, the inlet jet which flow speed was larger than 2.2 m/s was blanked. The molten steel jet penetrated the meniscus and impinged on the mold wall and flowed downward. Under the rotation of CCC system, the flow on meniscus rotated around. At the same casting speed, the increase of rotation speed from 40 rpm to 80 rpm caused little variation of gas entrainment (Fig.7a and 7b). Increasing casting speed from 1.27 m/min to 2.54 m/min induced more air entrainment into the strand, and a large amount of air bubble with various sizes penetrated more deeply (Fig.7a and 7c). The jet with higher energy impinged the meniscus seriously, causing meniscus fluctuation so that more air entrainment occurred.
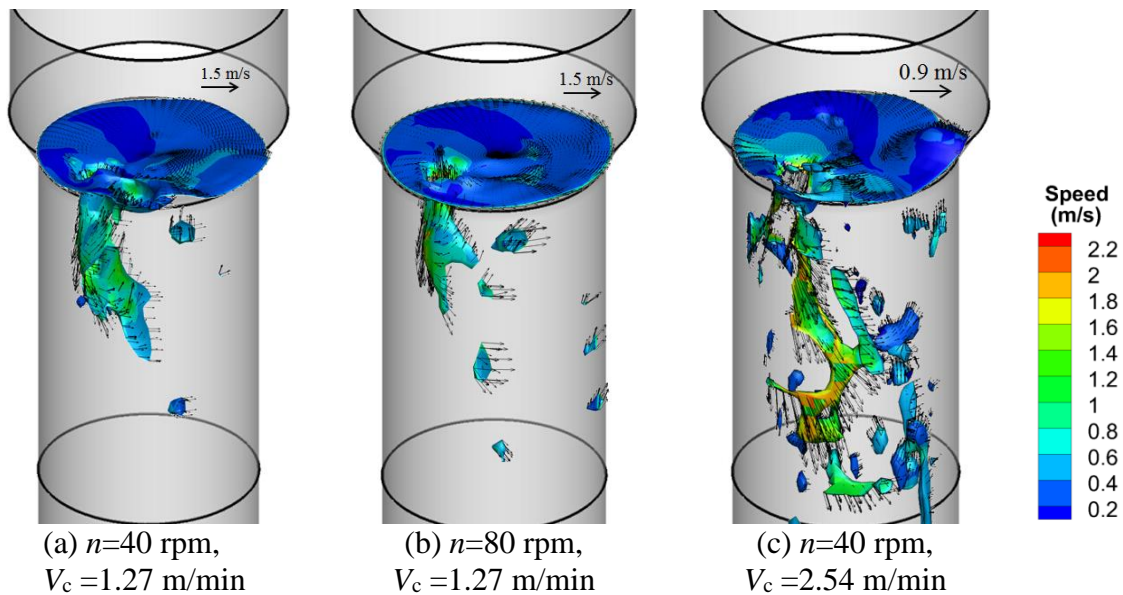

(a) *n*=40 rpm, V_c =1.27 m/min

(b) *n*=80 rpm, V_c =1.27 m/min

(c) *n*=40 rpm, V_c =2.54 m/min

Fig.7 Velocity vector at the interface between the molten steel and air phase (θ=8°)

(a) n=40 rpm,   (b) n=80 rpm,   (c) n=40 rpm,
V_c=1.27m/min V_c =1.27 m/min V_c =2.54 m/min
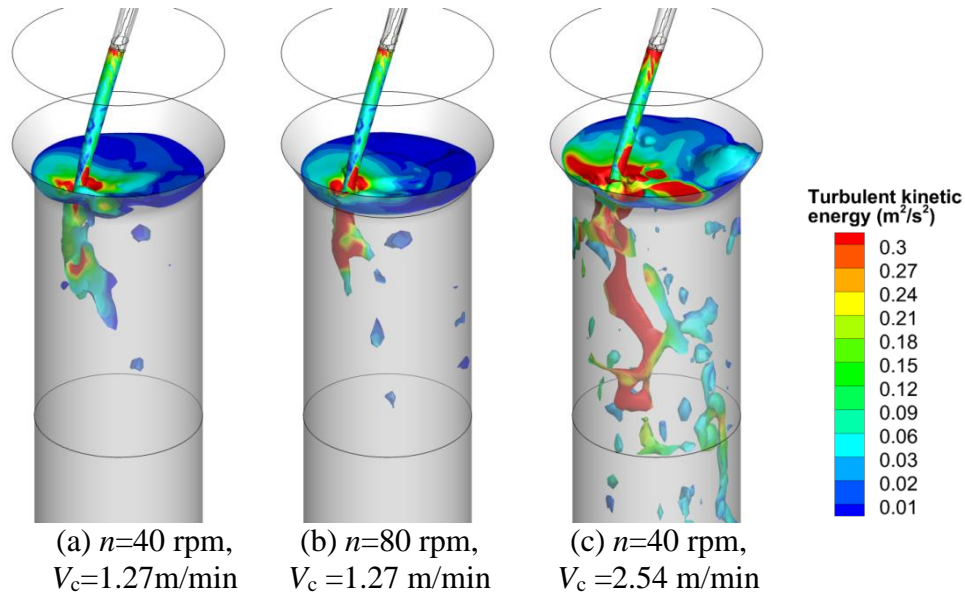
Fig.8 Distribution of k at the interface between the molten steel and air phase (θ=8°)

(a) n=40 rpm,   (b) n=80 rpm,   (c) n=40 rpm,
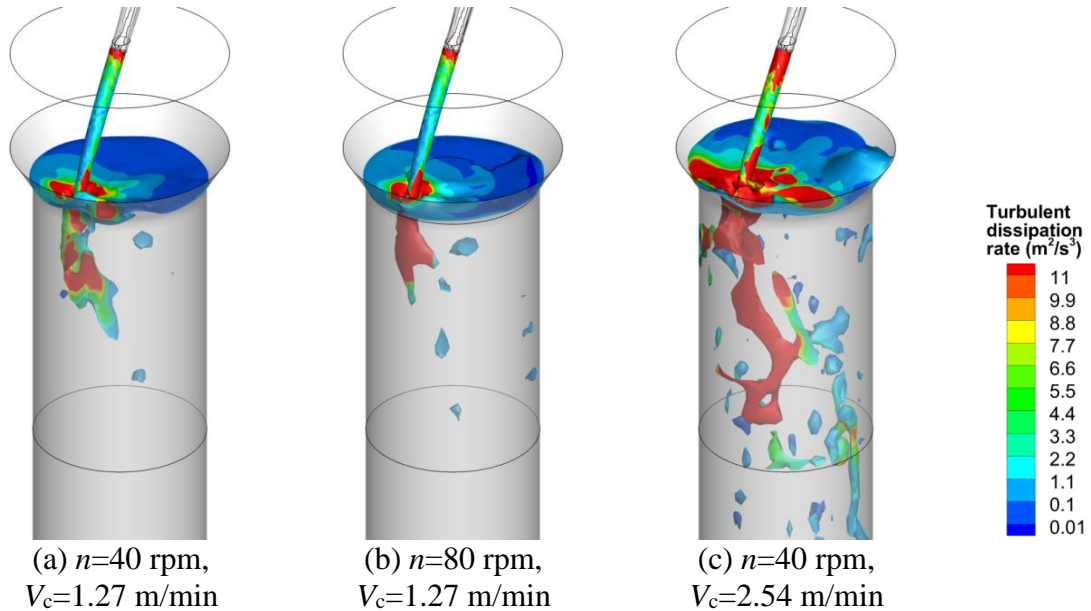V_c=1.27 m/min V_c=1.27 m/min V_c=2.54 m/min

Fig.9 Distribution of ε at the interface between the molten steel and air phase (θ=8°)

As k and ε were a measure of the intensity of turbulence, thus, could be directly related to the transport of momentum. The distributions of k and ε in Fig.8 and Fig.9 determined the ability of the flow to maintain turbulence or become turbulent. During pouring, larger k and ε of fluid flow mainly distributed on the impingement area of inlet jet and the surface of entrained gas. The increase of rotation speed has little influence on the flow stability on meniscus, while after increasing the casting speed twice, the obviously increased magnitude of k and ε indicated that the fluid flow on meniscus

became unstable.

Several typical streamlines inside the strand are shown in Figure 10. After the inlet jet impinged at the meniscus, swirls of various sizes were observed. The swirls inside the mold were large and complex, and the swirl at the meniscus was relatively small. As the distance below meniscus increased, the fluid flow tended to become rotational flow.
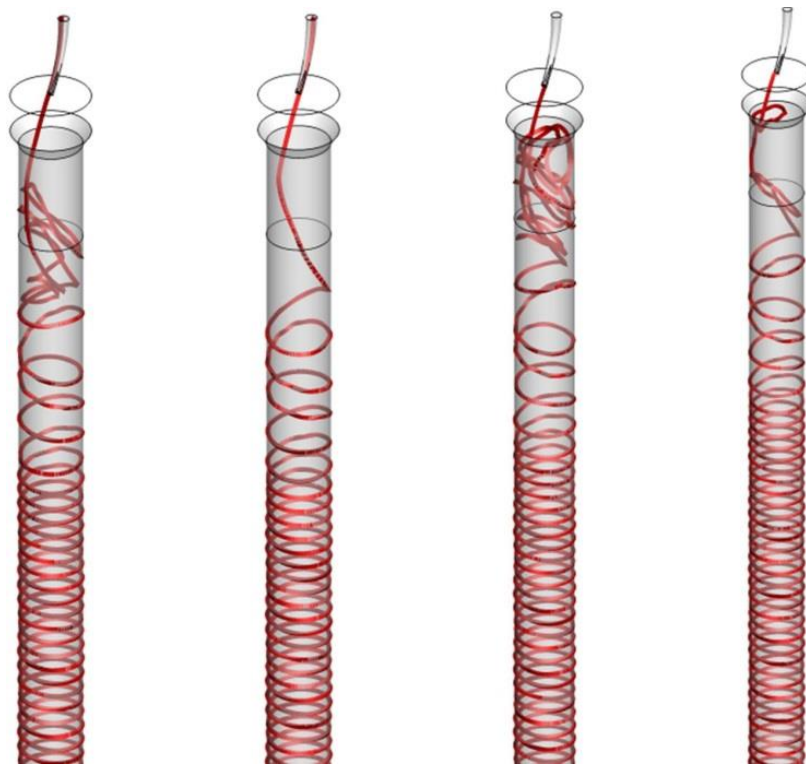

Fig.10 Streamlines inside the strand ($\theta=8°$, $n=40$ rpm, $V_c=1.27$ m/min)

Velocity vectors in vertical section and cross section planes are given in Figure 11. The inlet jet with high velocity impinged on the mold wall, resulting in level fluctuation at the interface of molten steel and gas. The flow inside the mold also was stirred by the flow jet. An overall rotation flow pattern was observed from the cross section planes. Due to the perturbation of the inlet jet, on the cross section 100 mm below the meniscus, the molten steel still flowed towards the mold wall. With the increasing of the distance below the meniscus, the rotation flow pattern became uniform more and more, and the location of the vortex gradually moved away from the mold wall.
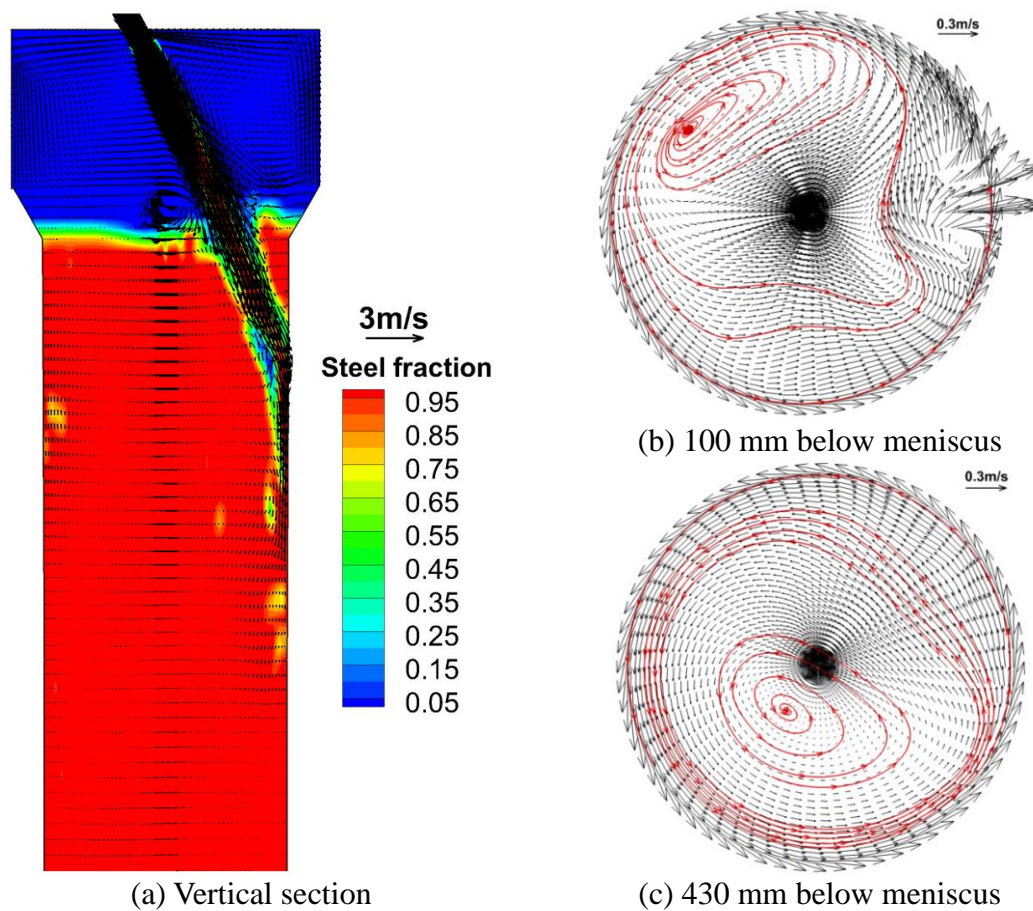
(a) Vertical section

(b) 100 mm below meniscus

(c) 430 mm below meniscus

Fig.11 Velocity vectors on different cross section planes (l=100 mm, n=40 rpm, V_c=1.27 m/min)

The flow speed along the vertical line 5 mm to the side of mold wall is compared in Figure 12. Fig.12a indicates that the flow speed varied violently in the mold region, and then became stable more and more with the increase of the distance below meniscus. In addition, the higher the rotation speed, the higher the flow speed. The increase of casting speed had a great influence on the flow within the mold region shown in Fig.12b, but little influence on the flow when the depth was over 1.5 m below meniscus.

(a) Effect of rotation speed (b) Effect of casting speed
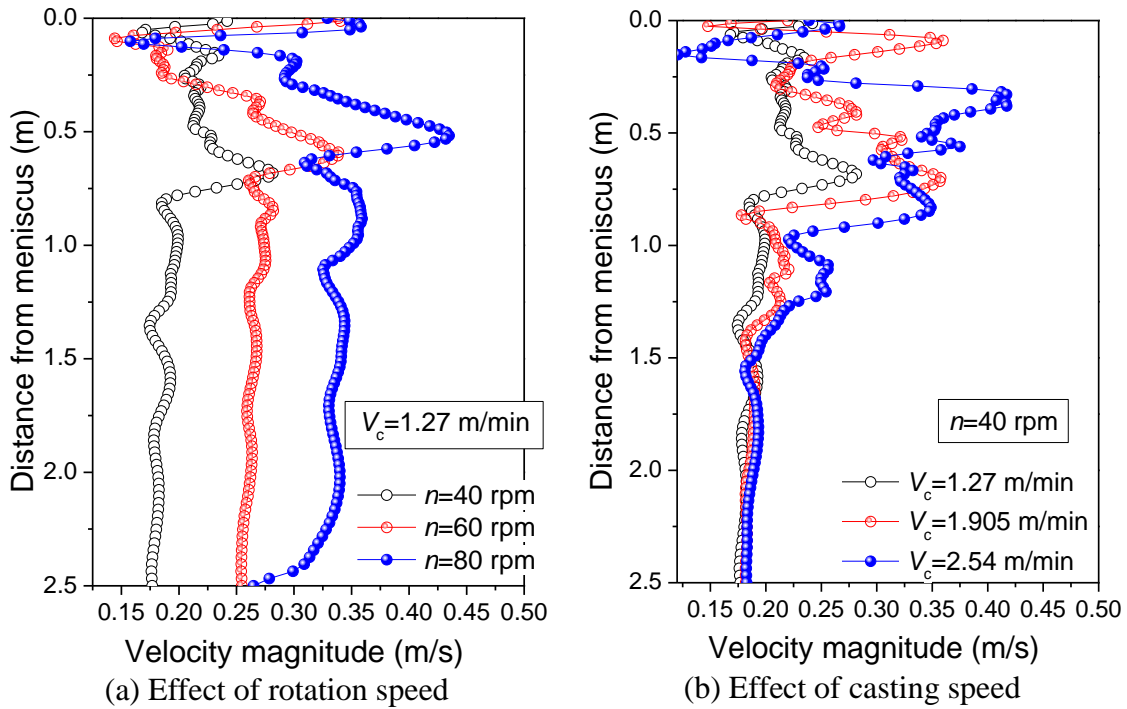
Fig.12 Comparison of speed near the left side of the mold wall

B. *Centrifugal Force*

Figure 13 shows the calculated centrifugal force on the cross section plane 15 m below meniscus. The centrifugal force was about 2500 N/m^3 close to mold wall, larger than other places. The greater the distance to the mold wall, the smaller the centrifugal force. And the centrifugal force near the center was below 100 N/m^3.
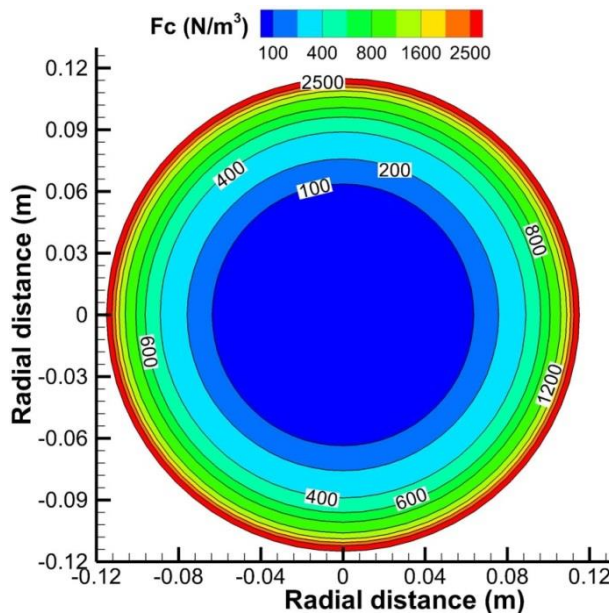

Fig.13 Calculated centrifugal force on the cross section plane 15 m below meniscus
(θ=8°, n=40 rpm, V_c=1.27 m/min)

The calculated centrifugal forces along one diameter on the cross section plane 15 m below meniscus under different casting conditions are shown in Figure 14. Horizontally and angularly moving the nozzle, and casting speed had little effect on the centrifugal force, the force was about 2500 N/m^3 at mold wall, and decreased sharply within 65 mm. The centrifugal force at the center was nearly zero, as shown in Fig.14a, 14b and 14d. The rotation speed has a significant effect on the centrifugal force. Increasing the rotation speed from 40 rpm to 80 rpm increased the maximum centrifugal force near the mold wall from 2600 N/m^3 to 9500 N/m^3 (Fig.14c).

(a) Distance of nozzle moving left
(l in Fig.5a)

(b) Angular moving angle of nozzle
(θ in Fig.5b)

(c) Rotation speed

(d) Casting speed
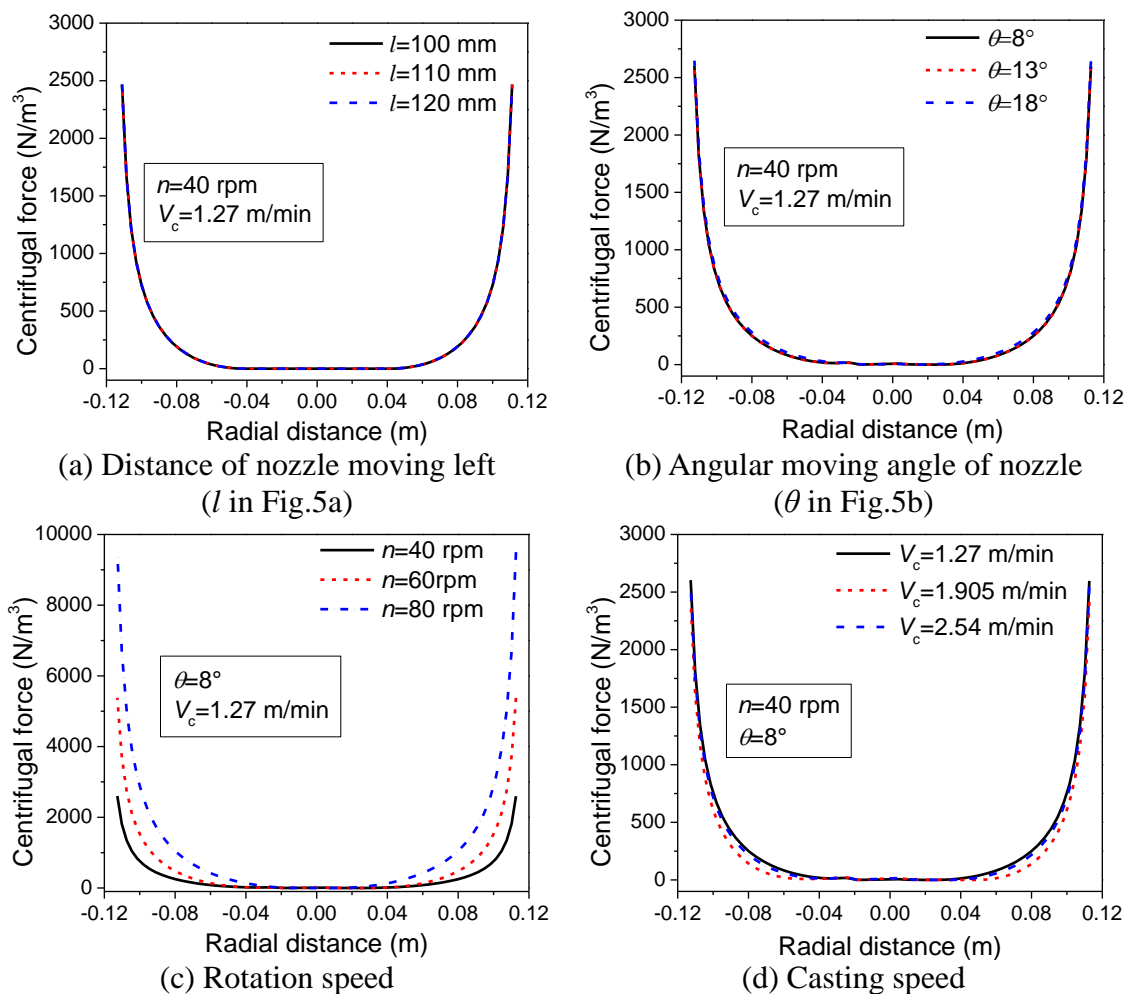
Fig.14 Calculated centrifugal forces under different casting conditions 15 m below meniscus

Practically, for horizontal centrifugal tube casting, to produce better quality hollow

tubes, the mold has to be accelerated to a certain rotation speed. Only with an optimum rotation speed, can the whole of the melt in the mold be picked up and held firmly against the mold wall and result in the formation of a uniform thickness tube which subsequently solidifies [49]. However, a rotation speed below a critical value or above an excessive value may lead to poor casting quality. With a rotation speed below the critical value, the liquid fails to form a cylinder with uniform thickness. Excessive rotation speed generally leads to inadmissible strong vibrations, which may result in longitudinal cracks caused by the hoop stress in the initial solidified shell [50]. The key operation is to determine the optimum rotation speed which generates appropriate centrifugal force.

For vertical CCC, the rotation speed is also a significant casting. Large rotation speed will cause the molten steel to splash and may affect the formation of initial shell. Hence, the choice of rotation speed should be paid more attention considering the smooth casting and the microstructure of billet.

C. *Level Fluctuation*

Figure 15 shows the three-dimensional time-varying level profiles post-processed. The negative value on the legend means the local level is below the original meniscus position. The inlet jet generated a deep depression of the level after impinging on the meniscus. Due to the lift of the upward flow, the level position near the mold wall was higher than the original meniscus position. At different computational times, the level had varied profile. In the current study, the penetration depth was defined as the vertical distance from the lowest point of level profile to the original meniscus position. As shown in Fig.15, at different times, the penetration depth was 121 mm, 125 mm, 130 mm and 123 mm, respectively.
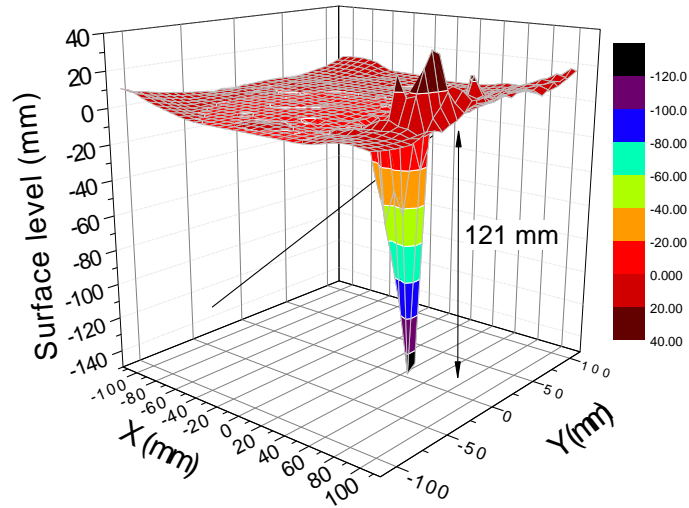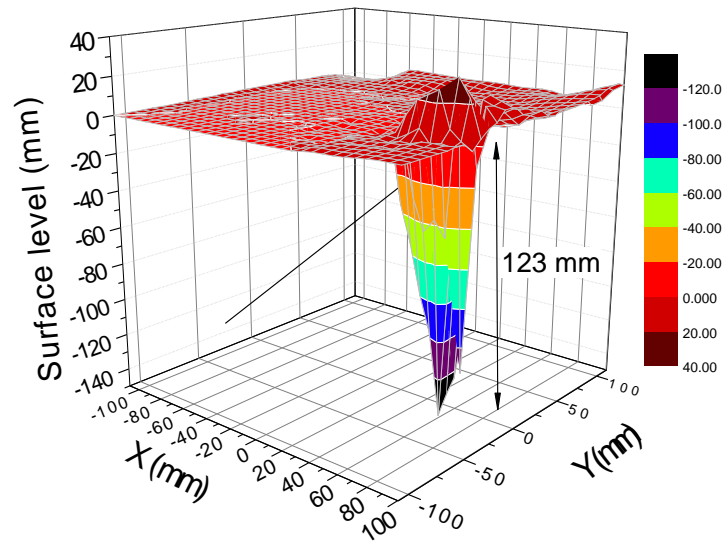
(a) time=16 s
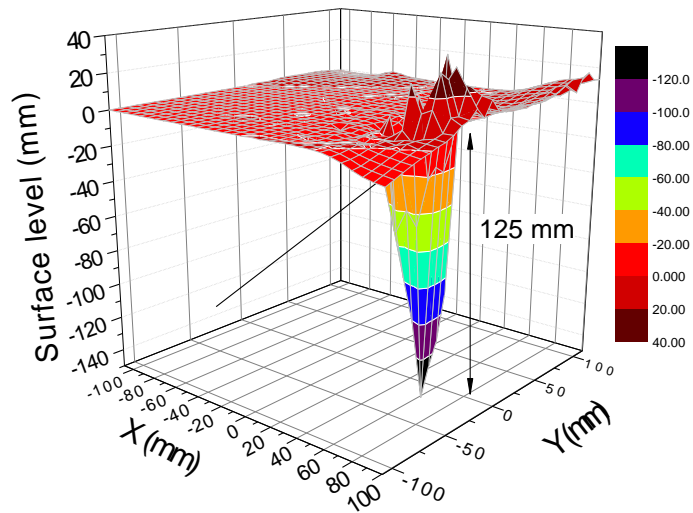
(c) time=17 s
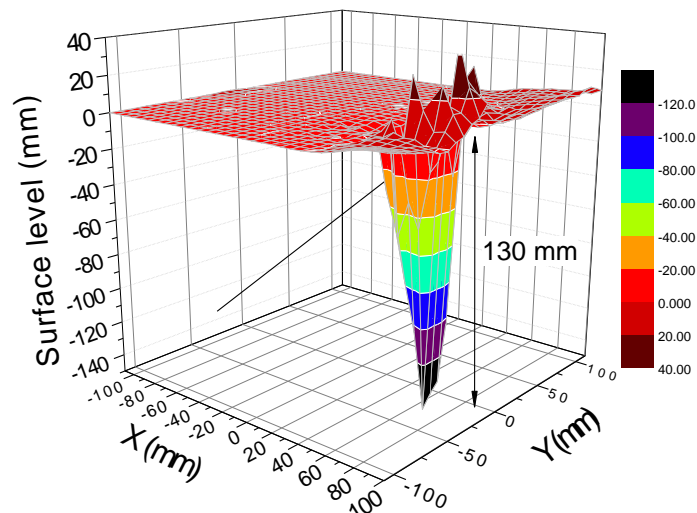
(c) time=18 s

(d) time=19 s

Fig.15 Level profiles at different computational time ($\theta=8°$, $n=40$ rpm, $V_c=1.27$ m/min)

The three-dimensional time-averaged level profiles of ten seconds with different angular moving distances are shown in Figure 16. When the angular angle of nozzle was 8°, the penetration depth was smallest with 113 mm. After increasing the angle from 8° to 18°, the penetration depth increased sharply from 113 mm to 174 mm. A larger penetration depth implies more air entrainment.
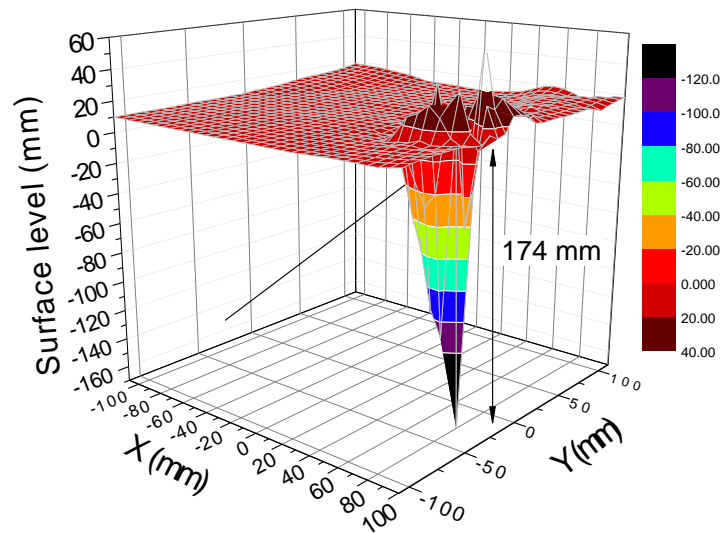

(a) $\theta=8°$

(b) θ=13°
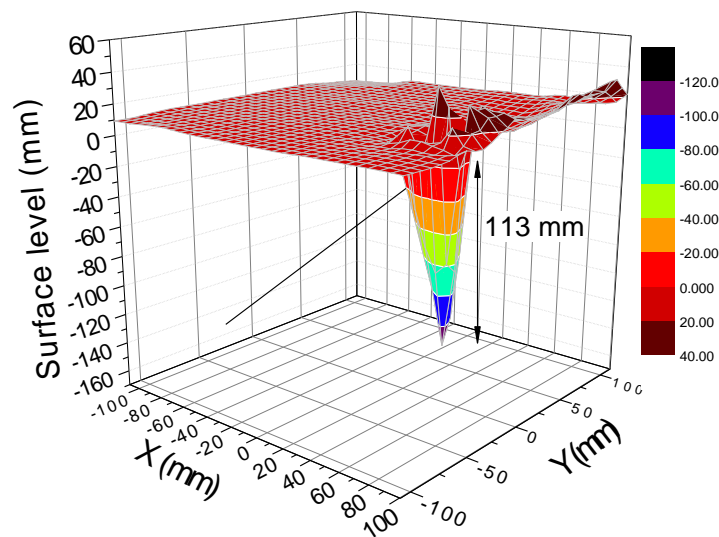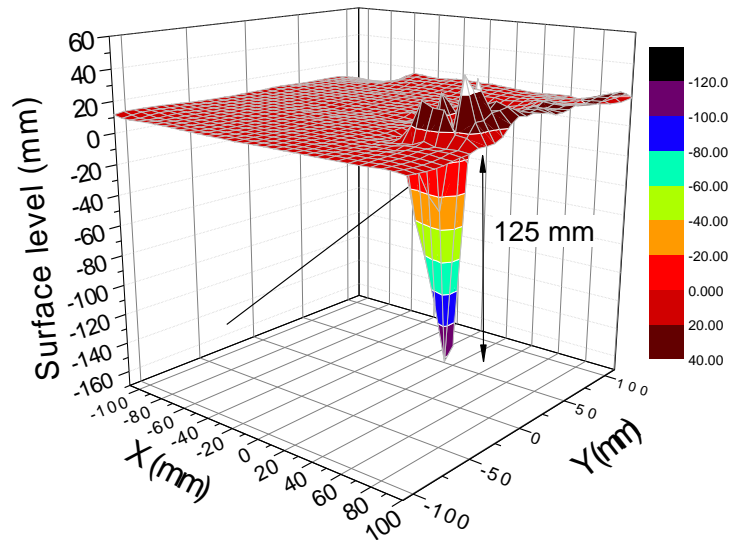
(c) θ=18°

Fig.16 Time-averaged level profiles with different angular angles of nozzle (n=40 rpm,

V_c=1.27 m/min)

Figure 17 illustrates the variation of the two-dimensional time-averaged level position of ten seconds when the nozzle moved left. The inlet jet generated a deep depression on the meniscus, over 110 mm below the meniscus. As the nozzle moved left, from 100 mm to 120 mm, the location of the depression moved towards the central area, and moving 110 mm left generated largest penetration depth.
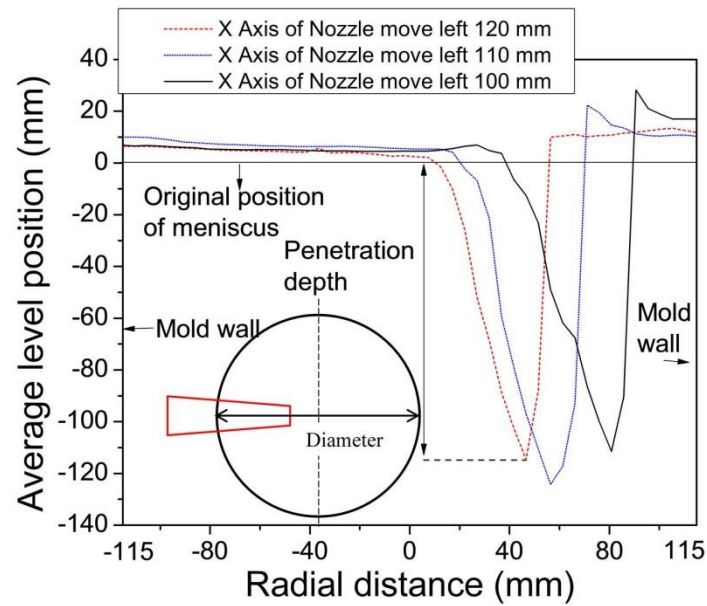
Fig.17 Effect of nozzle horizontal position on level shape of the mold

During centrifugal continuous casting, the rotation speed is an important parameter due to inducing the centrifugal force for the molten steel. Figure 18 revealed that with the same nozzle position (8° angular angle of nozzle) and casting speed (1.27 m/min), the rotation speed had little influence on the location of impact of the jet at the meniscus (Fig.18a). The penetration depth decreased slightly from 126 mm to 120 mm while the rotation speed increased from 40 rpm to 60 rpm, however, it increased distinctly from 120 mm with 60 rpm rotation speed to 178 mm with 80 rpm rotation speed. Hence, there exists a "critical rotation speed", exceeding which the level fluctuation becomes violent. If other parameters keep constant, higher casting speed implies higher molten steel flux into the mold. High continuous casting speed improves productivity and reduces energy consumption, but it may result in quality problems, such as severe surface fluctuation [17]. As shown in Fig.18b, after increasing the casting speed twice, the penetration depth was almost doubled from 126 mm to 220 mm.
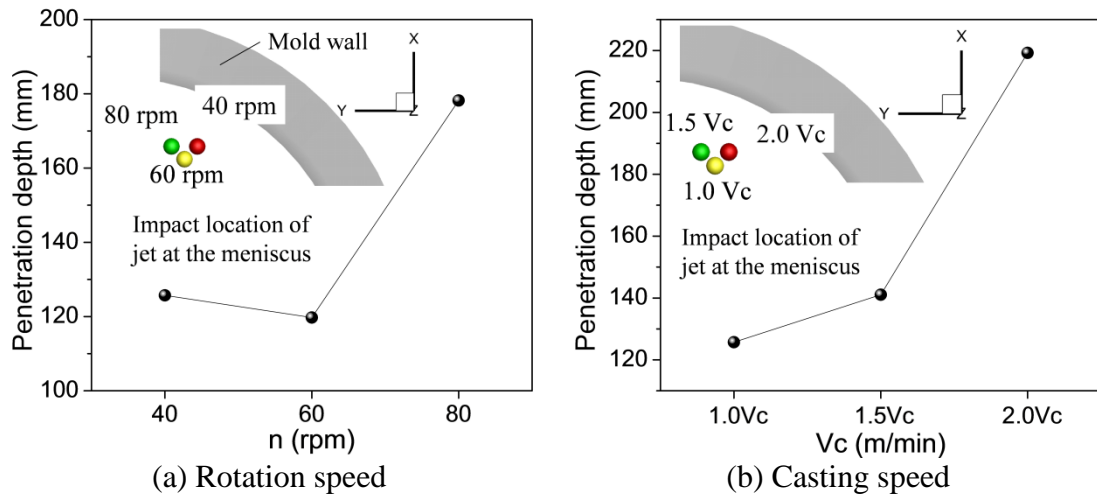
(a) Rotation speed   (b) Casting speed

Fig.18 Effect of rotation speed and casting speed on the penetration depth and impact location of jet at the meniscus

D. *Gas Entrainment into the Molten Steel*

During pouring, a large amount of gas was entrained into the molten steel, small bubbles could coagulate into larger ones. While larger bubbles might be broken up into small ones. The growth and broke-up of bubbles near the exit of mold at different times are shown in Figure 19.
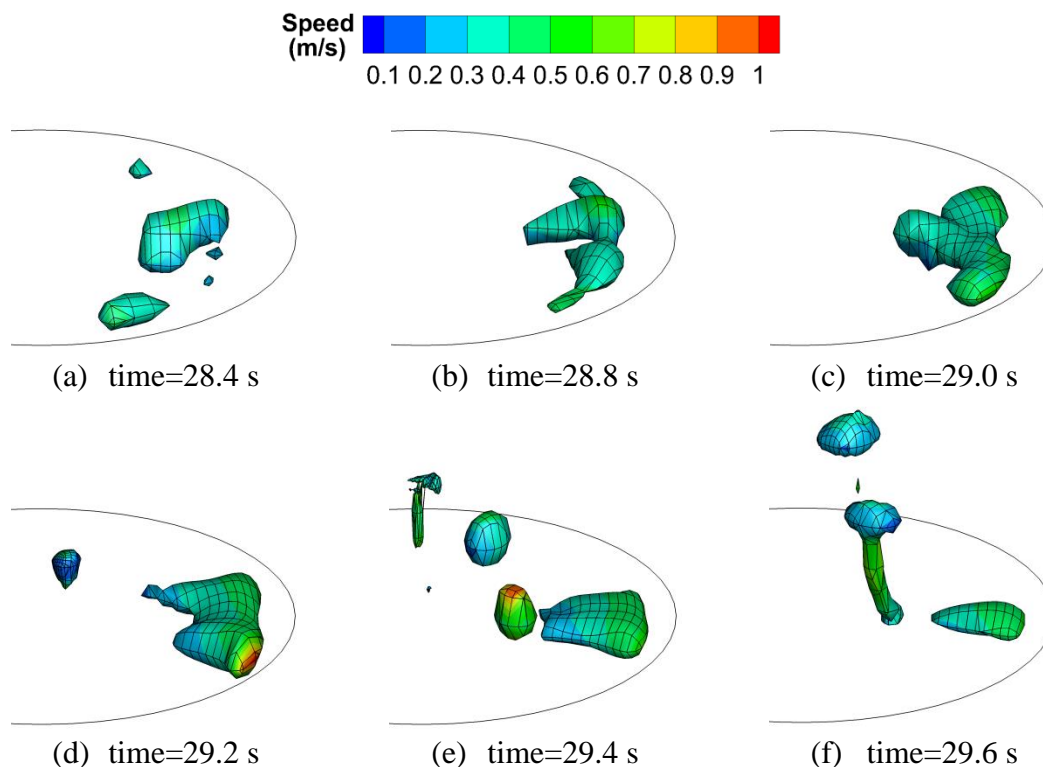

(a) time=28.4 s   (b) time=28.8 s   (c) time=29.0 s

(d) time=29.2 s   (e) time=29.4 s   (f) time=29.6 s

Fig.19 Growth and break-up of bubbles (θ=8°, n=40 rpm, V_c=1.27 m/min)

As shown in Fig.7, entrained bubbles can float upward and escape from the top of the mold. In actual practice, bubbles beneath the top surface of the molten steel are likely to be entrapped by the solidifying shell, eventually leading to defects such as surface slivers, blisters or internal defects in the rolled product [43]. Hence, to evaluate gas entrainment, the gas volume below the top surface, calculated by Eq.(10) was exported at each time step during calculation.

Figure 20 shows the volume of the entrained bubbles with casting time. Besides floating, bubbles were entrained into the molten steel and broken into many small ones. Hence, the variation of the volume of entrained bubbles fluctuated with time. Figure 21a shows as the nozzle moved left from 100 mm to 120 mm, the average volume of entrained bubbles increased from 0.00039 m³ to 0.00042 m³. Increasing angular moving angle of the nozzle and rotation speed resulted in a drop of the average volume of entrained bubbles, as shown in Fig.21b and 21c. As expected, higher casting speed led to more bubbles entrained into the molten steel (Fig.21d).
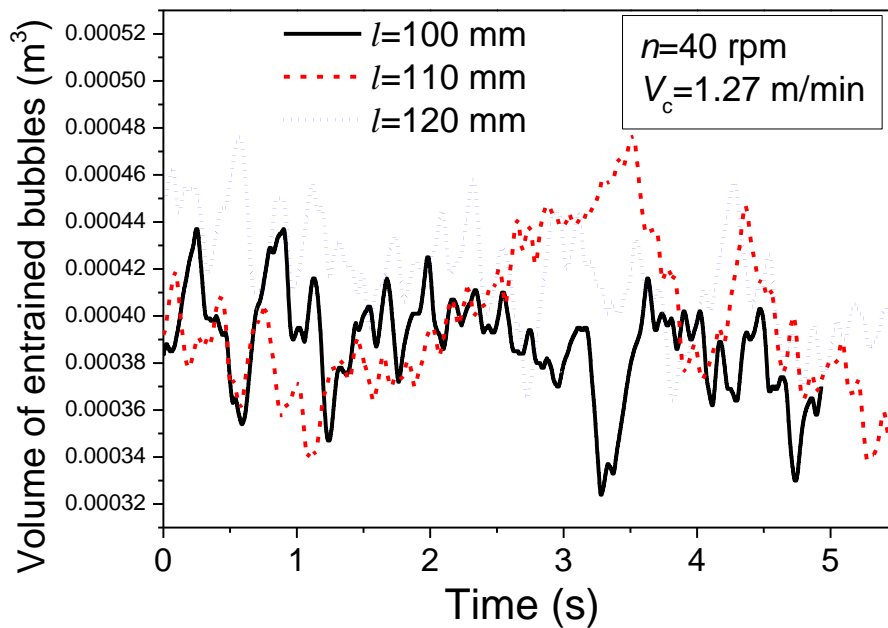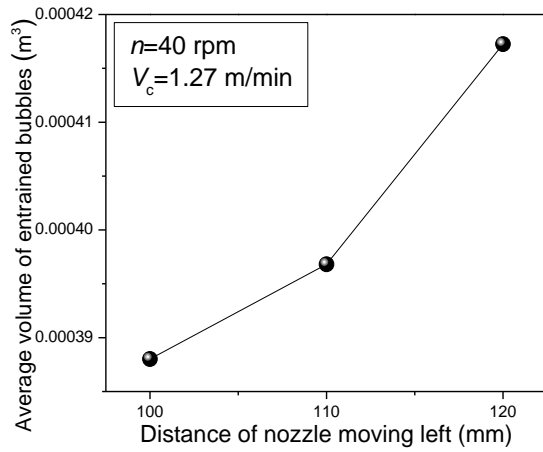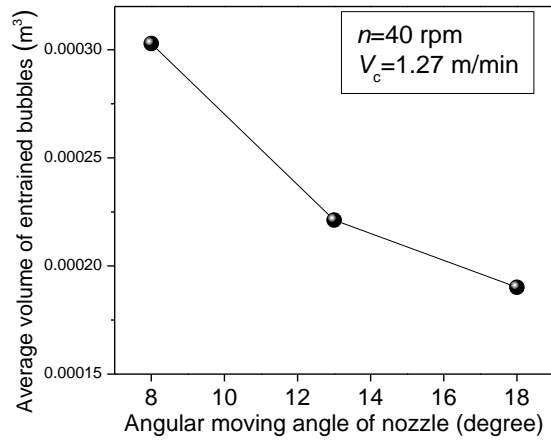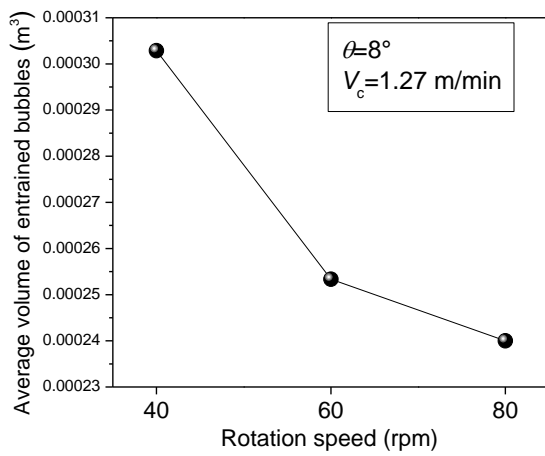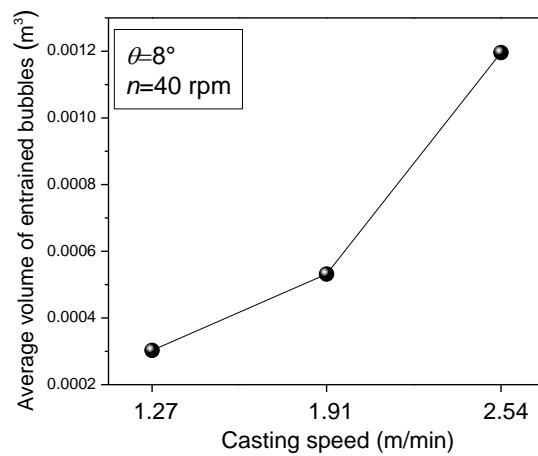

Fig.20 Volume of entrained bubbles with time

(a) Distance of nozzle moving to left
(l in Fig.5a)

(b) Angular moving angle of nozzle
(θ in Fig.5b)

(c) Rotation speed

(d) Casting speed

Fig.21 Influence of different parameters on the average volume of entrained bubbles

E. *Shear Stress on Mold Wall*

During continuous casting, a large shear stress on the solidified shell may cause uneven shell growth, and even induce the breakout. Since the current study focused on the turbulent flow and ignored the solidification, the shear stress on mold wall could represent it on the shell. Figure 22 shows the distribution of shear stress on mold wall. The maximum shear stress and the area fraction with shear stress >50 MPa are summarized in Figure 23. The maximum shear stress gradually decreased as the nozzle moved to the left in Fig.23a. The increase of angular moving angle of nozzle and casting speed caused an increase of shear stress on mold wall, as shown in Fig.23b and 23d. With 60 rpm rotation speed, the shear stress on mold wall was relatively large (Fig.23c)

(a) *l*=100mm　　　(b) *l*=110mm　　　(c) *l*=120mm
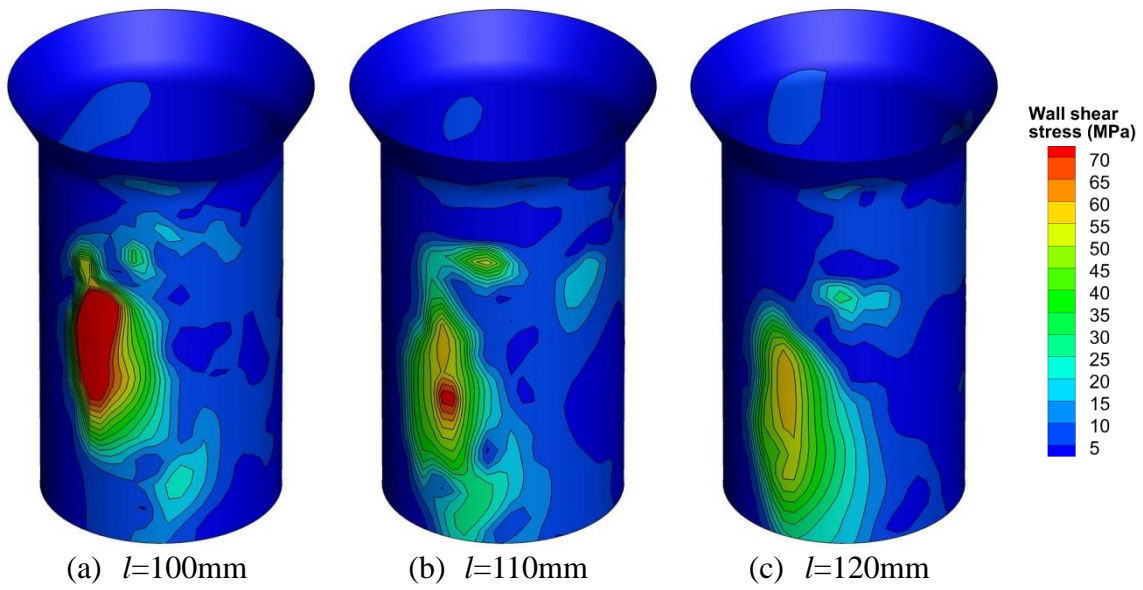
Fig.22 Distribution of shear stress on mold wall with different distance of nozzle moving left

(a) Distance of nozzle moving to the left
(*l* in Fig.5a)

(b) Angular moving angle of nozzle
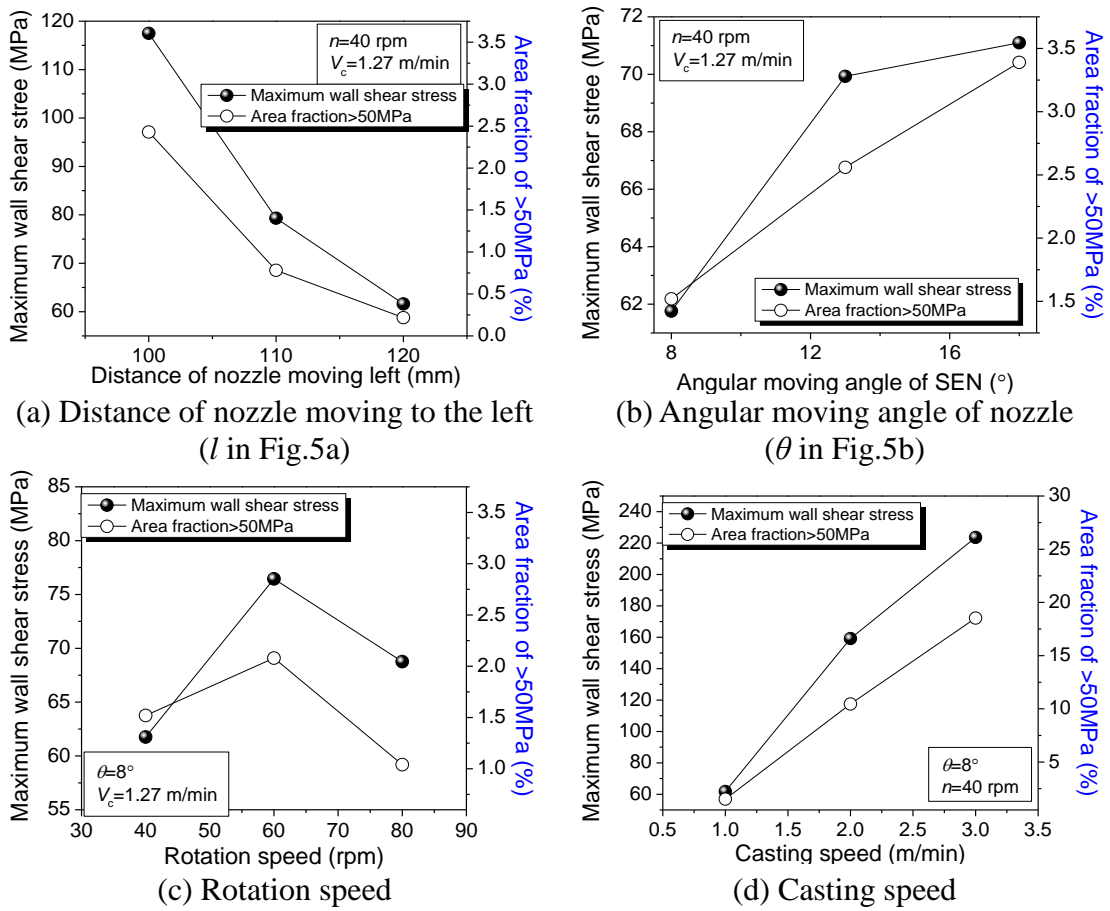(θ in Fig.5b)

(c) Rotation speed

(d) Casting speed

Fig.23 Influence of different parameters on the shear stress on mold wall

F. *Motion of Inclusions during CCC*

To illustrate the centrifugal effect, the motion of inclusions in the strand was investigated. The initial locations of inclusions were uniformly distributed on the surface of nozzle inlet, and the initial velocity of inclusions was local fluid flow velocity. Five thousand inclusions of each size were released after the fluid flow reached steady state. Figure 24 shows the calculated random trajectories of inclusions with different diameters. The particles entered into the mold with the flow jet, and due to the effect of turbulent fluid on the motion of inclusions, the trajectories of inclusions in the mold region were irregular. Then under the influence of rotation flow, the inclusions also rotated along the strand length. After moving a certain distance along the casting direction, the inclusions gradually moved to the center of billet, and the behavior of rotation for inclusions became weak. It seems that larger particles penetrated and circulated more deeply than the smaller ones.
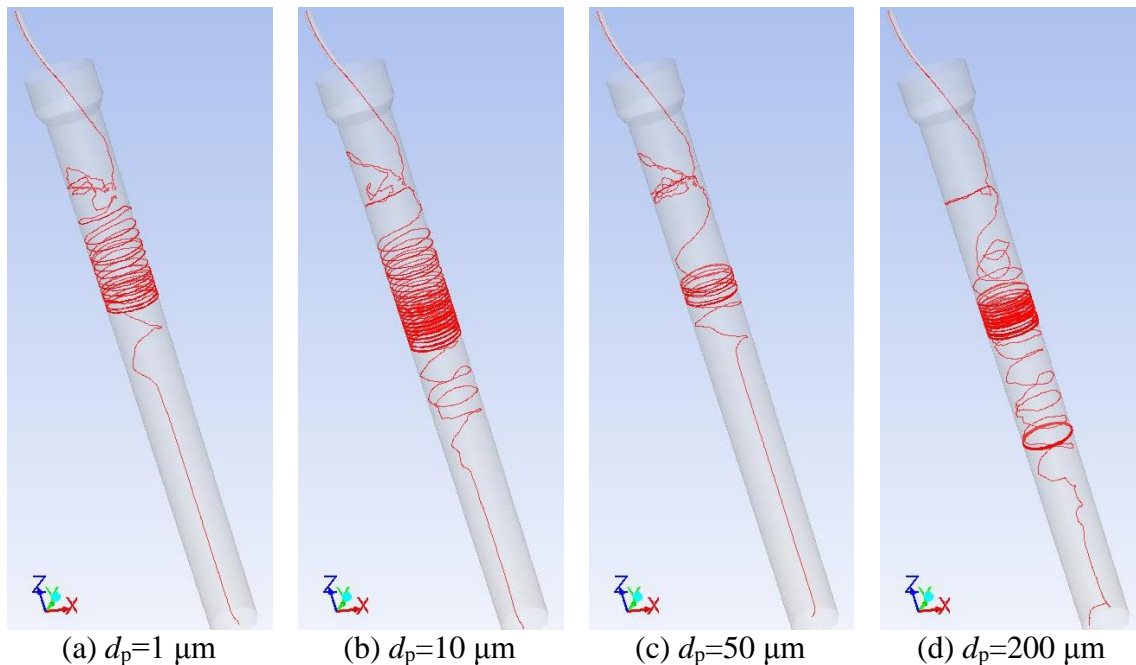

(a) d_p=1 μm   (b) d_p=10 μm   (c) d_p=50 μm   (d) d_p=200 μm

Fig.24 Random trajectories of inclusions with different diameters (*l*=100 mm, *n*=40 rpm, V_c= 1.27 m/min)

The effect of F_c in Eq. (9) on the distribution of inclusions was discussed by analyzing the number of inclusions along the diameter on the cross section plane 15 m below meniscus. The analysis area was divided into twenty-three 10 mm×10 mm squares, as shown in Figure 25.
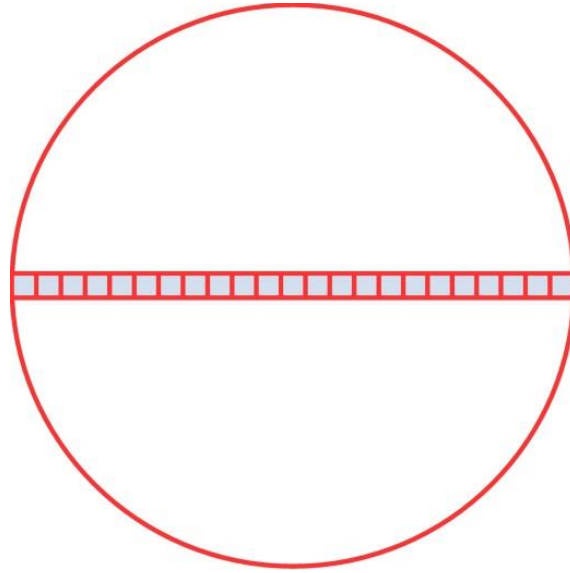

Fig.25 Schematic of analysis area

The distributions of the number of inclusions with different diameters are given in Figure 26. On the whole, the number of inclusions gradually increased from the outer radius of the billet to the center. The addition of F_c made more inclusions gather at the center, especially for 200 μm inclusions. Hence, in order to predict the trajectories more accurately, F_c would be taken into account in the current study.

(a) 1 μm inclusions   (b) 10 μm inclusions
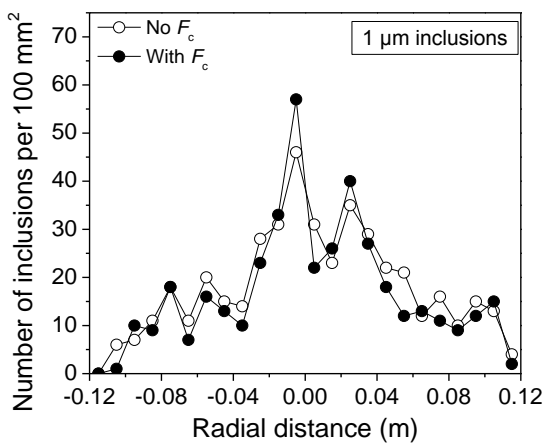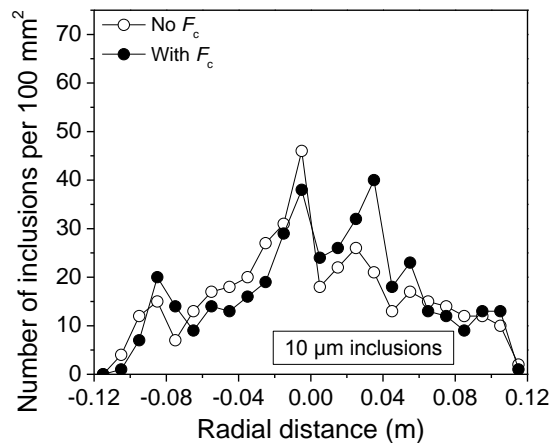
(c) 50 μm inclusions   (d) 200 μm inclusions

Fig.26 Number of inclusions with different diameters per 100 mm^2

The locations of typical small and large inclusions passing the cross section plane 1 m below the meniscus were projected to a two-dimensional figure, as shown in Figure 27.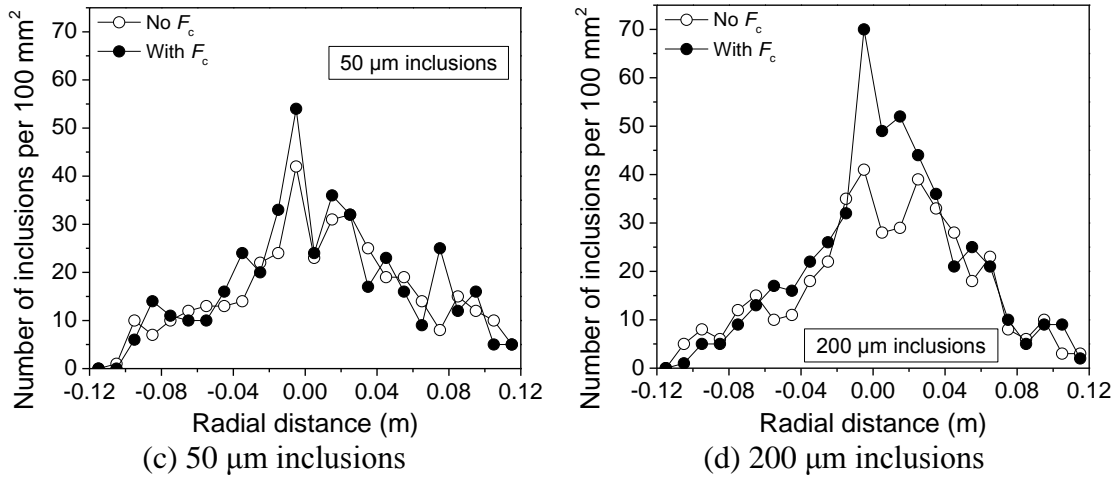 Indicating that the distribution of inclusions was nonuniform, and many gathered near the side wall. Comparing to the fluid flow in Fig.11, it can be seen that the locations of inclusions were mainly determined by the turbulent fluid flow and the distribution of inclusions confirmed the feature of CCC. As inclusions became large, more of them distributed close to the central area, since larger centrifugal force exerted on larger inclusions toward the center. Hence, smaller inclusions would be entrapped within the outer radius of the billet, while larger ones would be pushed to the center of the billet.

Figure 28 shows the locations of 1 μm inclusions at four cross section planes along casting direction. At the cross section plane 1m below meniscus, inclusions mainly distributed near the side. At the cross sections planes of 6 m and 11 m below meniscus, most inclusions were entrapped around the center area. Since the solidification was ignored in the current study, the position of inclusions was mainly determined by the turbulent fluid flow.

(a) 50 μm inclusions　　　　　　　　(b) 200 μm inclusions
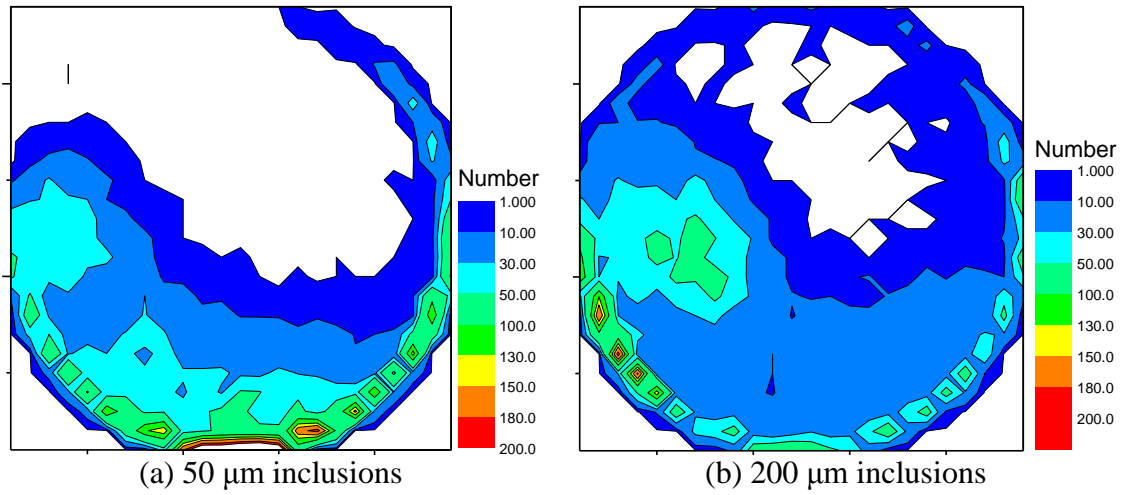
Fig.27 Location of inclusions passing the cross section plane 1 m below meniscus (θ=8°, n=40 rpm, V_c=1.27 m/min)
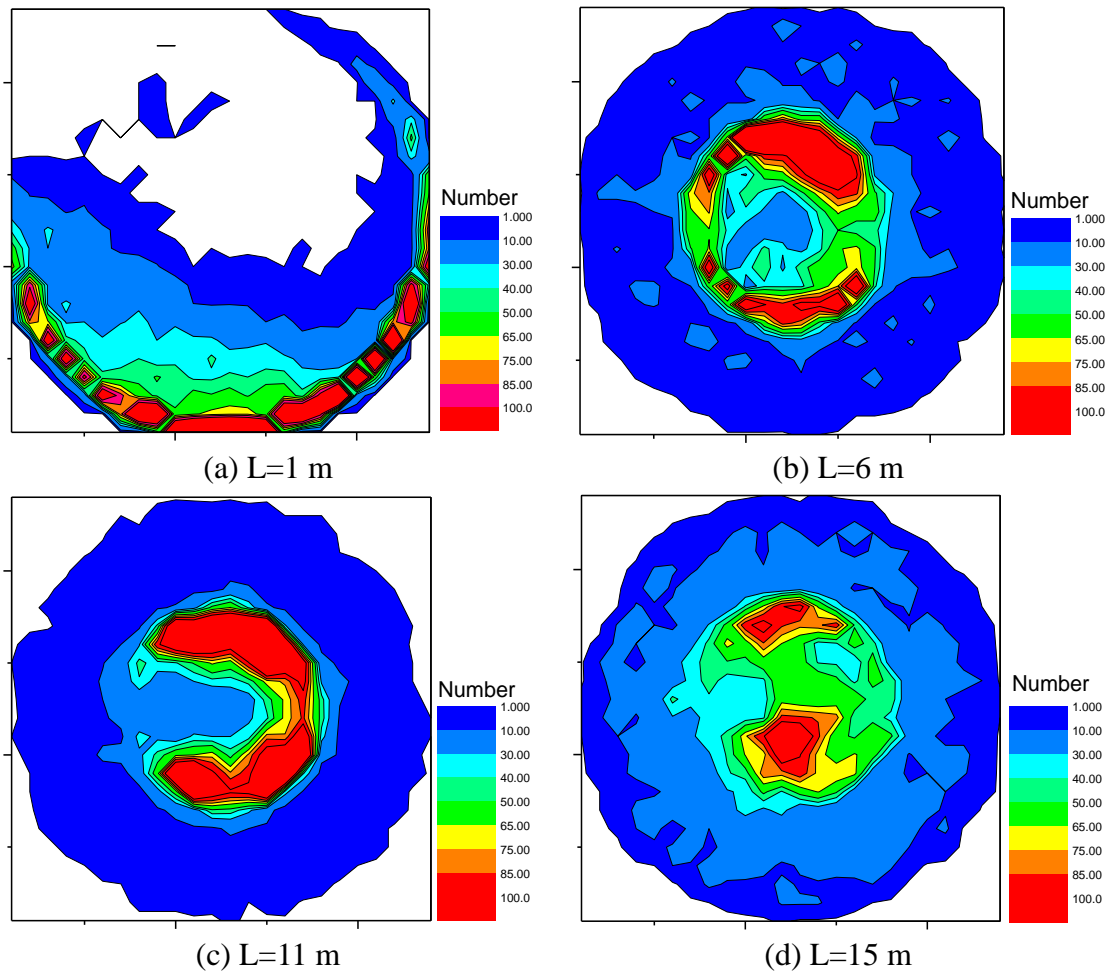

(a) L=1 m　　　　　　　　　　　(b) L=6 m

(c) L=11 m　　　　　　　　　　　(d) L=15 m

Fig.28 Location of 1 μm inclusions passing cross section planes different distance below meniscus (θ=8°, n=40 rpm, V_c=1.27 m/min)

The influence of casting parameters on the distribution of inclusions was represented by the index, N/N_0, where N_0 was the maximum number of inclusions among the squares, and N was the number of inclusions at each square in Fig.25. The index of the number of inclusions under various conditions was shown in Figure 29. Comparing Fig.29a and 29b, with the increase of the angular angle of nozzle from 8° to 18°, the distribution of inclusions became more dispersed, as the index of the number of inclusions increased generally. Fig.29a and 29c indicated that more inclusions would aggregate at higher casting speed, and the inhomogeneity of inclusions across the section became more serious. The increase of rotation speed had little influence on the distribution of inclusions, besides 1 μm inclusions which distribution was more dispersive (Fig.29d).

(a) V_c=1.27 m/min, θ=8°, n=40 rpm

(b) V_c =1.27 m/min, θ=18°, n=40 rpm

(c) V_c =2.54 m/min, θ=8°, n=40 rpm

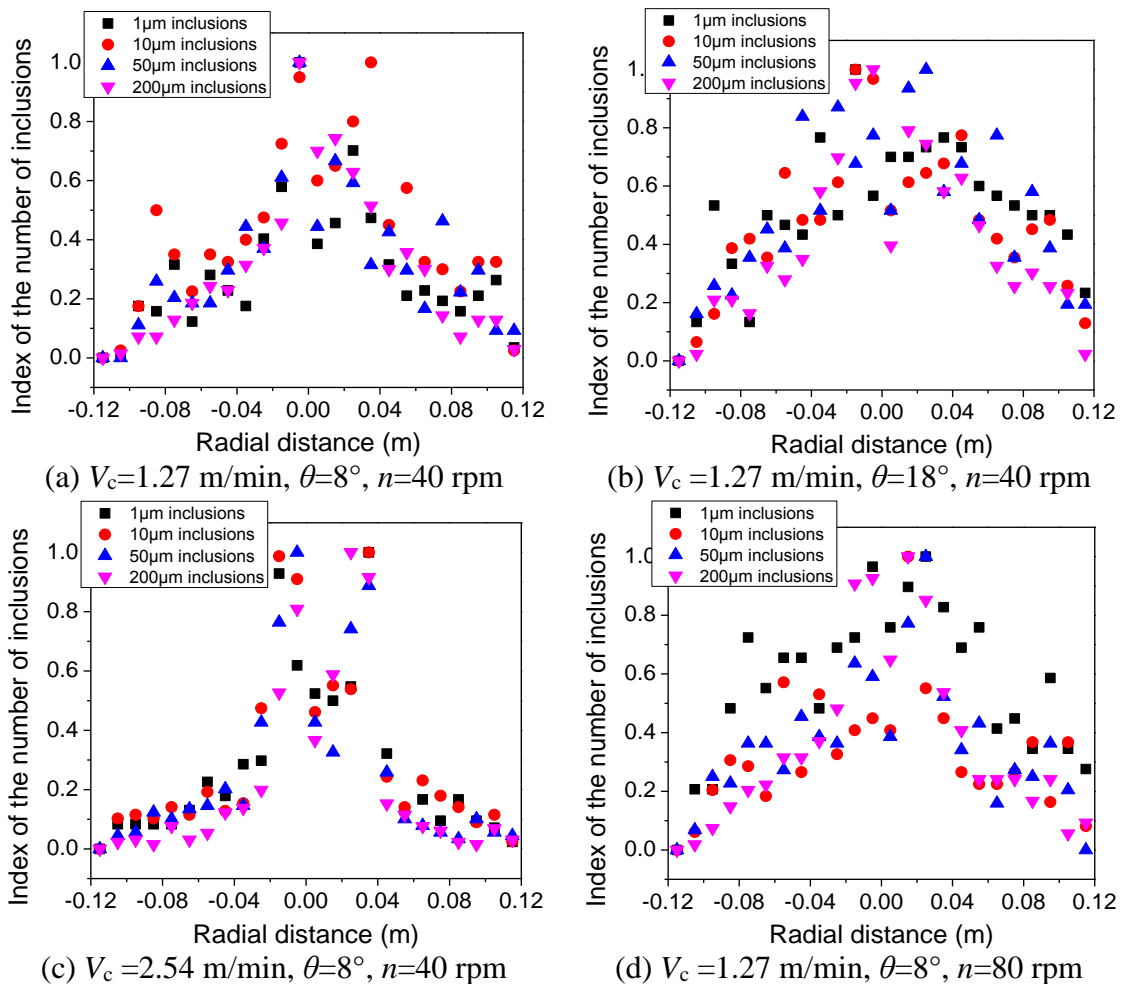(d) V_c =1.27 m/min, θ=8°, n=80 rpm

Fig.29 Influence of different parameters on the distribution of inclusions 15 m below meniscus

From the discussion above, it can be concluded that inclusions tended to accumulate in

the region close to the center of the billet by the effect generated by the centrifugal force. It occurred since the molten steel itself is denser than inclusions and under the action of centrifugal force, the denser steel is pushed to the outer region, forcing the lighter inclusions to the inner region. More study considering the effect of solidification on the entrapment of inclusions will be discussed in another paper[35] about the CCC process.

IV. CONCLUSIONS

A three-dimensional multi-phase turbulent model was established to study the transport phenomena during CCC process. Conclusions can be summarized as follow:

1) During pouring, a large amount of gas was entrained into the molten steel, and broken into bubbles of various sizes. And due to the rotating system, the stream within the fluid field flows around the side wall.

2) The greater the distance to the mold wall, the smaller the centrifugal force. Horizontally and angularly moving the nozzle, and casting speed had little effect on the distribution of centrifugal force, while increasing the rotation speed from 40 rpm to 80 rpm significantly increased the maximum centrifugal force near the mold wall from 2600 N/m^3 to 9500 N/m^3

3) When the nozzle moved left, the location of the depression at meniscus moved towards the central area, the penetration depth did not change much, about 115 mm. Angular moving angle of the nozzle with 8° and keeping the rotation speed with 60 rpm could somehow stabilize the level fluctuation.

4) Due to the entrainment and break-up of bubbles, the variation of the volume of entrained bubbles fluctuated with time. The increase of angular angle of nozzle from 8° to 18° and rotation speed from 40 rpm to 80 rpm favored to decrease the total volume of entrained bubbles, while the increase of distance of nozzle moving left and casting speed had reverse effects.

5) As the nozzle moved left, the maximum shear stress gradually decreased. The increase of angular moving angle of nozzle and the increase of casting speed

caused an increase of shear stress on mold wall. The shear stress on mold wall was relatively large when the rotation speed was 60 rpm.

6) Under the rotating system, inclusions entering into the strand would gather near the center area of billet along casting direction. Different casting parameters had various effects on the distribution of inclusions on the cross section planes.

7) To discuss the effect of casting parameters on the heat transfer, solidification and inclusions entrapment during CCC, more work will be performed.

REFERENCES

[1]   B. D. Khakhalin, A. N. Smolyakov. Centrifugal casting of 50mm cast iron standpipes[J]. Metallurgist, 1957, 1(3): 176-178.

[2]   L. S. Konstantinov, B. D. Khokhalin, A. N. Smoliakov. Centrifugal casting of tubes in the People's Republic of China[J]. Metallurgist, 1958, 2(9): 495-497.

[3]   I. O. Tsypin, N. S. Pavlenko, V. A. Rusalkin. Wear resistance of high-strength cast iron with spheroidal graphite produced by centrifugal casting[J]. Metal Science and Heat Treatment, 1968, 10(9): 745-746.

[4]   G. Martinez, M. Garnier, F. Durand. Stirring phenomena in centrifugal casting of pipes[J]. Applied Scientific Research, 1987, 44(1-2): 225-239.

[5]   Charles B. Stravs, John N. Jager, Apparatus for forming pipe or other articles in continuous lengths, Office, Editor 1904: the United States.

[6]   George R. Leghorn, Continuous centrifugal casting of tube using liquid mold, 1971: the United States.

[7]   William H. Milispaugh, Centrifugal casting method, 1931: The United States.

[8]   J. Anagnostopoulos, G. Bergeles. Three-dimensional modeling of the flow and the interface surface in a continuous casting mold model[J]. Metallurgical and Materials Transactions B, 1999,

30(6): 1095-1105.

[9] A. Theodorakakos, G. Bergeles. Numerical investigation of the interface in a continuous steel casting mold water model[J]. Metallurgical and Materials Transactions B, 1998, 29(6): 1321-1327.

[10] Jun Aoki, Brian G. Thomas, Jorg Peter, Kent D. Peaslee. Experimental and theoretical investigation of mixing in a bottom gas-stirred ladle[A]. Proceedings of AISTech 2004 Conference[C]. 2004: 1045-1056.

[11] Lifeng Zhang. Mathematical simulation of fluid flow in gas-stirred liquid systems[J]. Modelling and Simulation in Materials Science and Engineering, 2000, 8(4): 463.

[12] Y. Xie, S. Orsten, F. Oeters. Behavior of bubbles at gas blowing into liquid Wood's Metal[J]. ISIJ International, 1992, 32(1): 66-75.

[13] J. E. Lait, J. K. Brimacombe, F. Weinberg. Mathematical modelling of heat flow in the continuous casting of steel[J]. Ironmaking and Steelmaking, 1974, 1(2): 90-97.

[14] C. W. Hirt, B. D. Nichols. Volume of fluid (VOF) method for the dynamics of free boundaries[J]. Journal of Computational Physics, 1981, 39(201-225.

[15] Brian G. Thomas, X. Huang, R. C. Sussman. Simulation of argon gas flow effects in a continuous slab caster[J]. Metallurgical and Materials Transactions B, 1994, 25(4): 527-547.

[16] Yeong-Ho Ho, Weng-Sing Hwang. The analysis of molten steel flow in billet continuous casting mold[J]. ISIJ International, 1996, 36(8): 1030-1035.

[17] G. A. Panaras, A. Theodorakakos, G. Bergeles. Numerical investigation of the free surface in a continuous steel casting mold model[J]. Metallurgical and Materials Transactions B, 1998, 29(5): 1117-1126.

[18] Lijian Tan, Houfa Shen, Baicheng Liu, Xiao Liu, Rongjun Xu, Yongquan Li. Numerical simulation of surface oscillation in continuous casting mold[J]. Acta Metallurgica Sinica, 2003, 39(4): 435-438.

[19] Lifeng Zhang, Yufeng Wang, Xiangjun Zuo. Flow transport and inclusion motion in steel continuous-casting mold under submerged entry nozzle clogging condition[J]. Metallurgical and Materials Transactions B, 2008, 39(4): 534-550.

[20] R. Chaudhary, Go-Gi Lee, Brian G. Thomas, Seon-Hyo Kim. Transient mold fluid flow with well- and mountain-bottom nozzles in continuous casting of steel[J]. Metallurgical and Materials Transactions B, 2008, 39(6): 870-884.

[21] Yufeng Wang, Lifeng Zhang. Transient fluid flow phenomena during continuous casting: part I-cast start[J]. ISIJ International, 2010, 50(12): 1777-1782.

[22] Yufeng Wang, Lifeng Zhang. Transient fluid flow phenomena during continuous casting: part II-cast speed change, temperature fluctuation, and steel grade mixing[J]. ISIJ International, 2010, 50(12): 1783-1791.

[23] Ismael Calderon-Ramos, José de Jesús Barreto, Saul Garcia-Hernandez. Physical and mathematical modelling of liquid steel fluidynamics in a billet caster[J]. ISIJ International, 2013, 53(5): 802-808.

[24] Brian G. Thomas, Lifeng Zhang. Mathematical modeling of fluid flow in continuous casting[J]. ISIJ International, 2001, 41(10): 1181-1193.

[25] Raul Mirandal, Miguel Angel Barron, Jose Barreto, Luis Hoyos, Jesus Gonzalez. Experimental and numerical analysis of the free surface in a water model of a slab continuous casting mold[J]. ISIJ International, 2005, 45(11): 1626-1635.

[26] Yufeng Wang, Lifeng Zhang. Fluid flow-related transport phenomena in steel slab continuous

casting strands under electromagnetic brake[J]. Metallurgical and Materials Transactions B, 2011, 42(6): 1319-1351.

[27]   Rui Liu, Brian G. Thomas, Bruce Forman, Hongbin Yin. Transient turbulent flow simulation with water model validation and application to slide gate dithering[A]. Proceedings of AISTech 2012 Conference[C]. 2012: 1317-1327.

[28]   Hugo Arcos-Gutierrez, Gerardo Barrera-Cardiel, Jose de Jesus Barreto, Saul Garcia-Hernandez. Numerical study of internal SEN design effects on jet oscillations in a funnel thin slab caster[J]. ISIJ International, 2014, 54(6): 1304-1313.

[29]   Lifeng Zhang, Brian G. Thomas. State of the art in evaluation and control of steel cleanliness[J]. ISIJ International, 2003, 43(3): 271-291.

[30]   S. Asai, J. Szekely. Turbulent flow and its effects in continuous casting[J]. Ironmaking and Steelmaking, 1975, 2(3): 205-213.

[31]   Quan Yuan, Brian G. Thomas, S. P. Vanka. Study of transient flow and particle transport in continuous steel caster molds: part II. particle transport[J]. Metallurgical and Materials Transactions B, 2004, 35(4): 703-714.

[32]   Dipak Mazumdar, Roderick I. L. Guthrie. Comparison of three mathematical modeling procedures for simulating fluid flow phenomena in bubble-stirred ladles[J]. Metallurgical Transactions B, 1994, 25(2): 308-312.

[33]   Alessio Alexiadis, Pascal Gardin, Jean Francois Domgin. Spot turbulence, breakup, and coalescence of bubbles released from a porous plug injector into a gas-stirred ladle[J]. Metallurgical and Materials Transactions B, 2004, 35(5): 949-956.

[34]   Lifeng Zhang, Qiangqiang Wang, Sridhar Seetharaman, Wen Yang, Yi Wang, Shufeng Yang. Detection of Non-metallic Inclusions in Centrifugal Continuous Casting Steel Billets[J]. 2015,

[35]   Qiangqiang Wang, Lifeng Zhang. Determination for the entrapment criterion of non-metallic inclusions by the solidification front during steel centrifugal continuous casting[J]. 2015,

[36]   Rui Liu, Brian G. Thomas, Love Kalra, Tathagata Bhattacharya, Aloka Dasgupta. Slidegate dithering effects on transient flow and mold level fluctuations[A]. Proceedings of AISTech 2013 Conference[C]. 2013: 1351-1364.

[37]   B. E. Launder, D. B. Spalding. Number computation of turbulent flows[J]. Computer Methods in Applied Mechanics and Engineering, 1974, 3(2): 269-289.

[38]   Brian G. Thomas, Quan Yuan, Sivaraj Sivaramakrishnan, Tiebiao Shi, S. P. Vanka, Mohammad B. Assar. Comparison of four methods to evaluate fluid velocities in a continuous slab casting mold[J]. ISIJ International, 2001, 41(10): 1262-1271.

[39]   B. E. Launder, D. B. Spalding. Mathematical models of turbulence[M]. New York: Academic Press, 1972.

[40]   Yeong-Ho Ho, Chi-Hung Chen, Weng-Sing Hwang. Analysis of molten steel flow in slab continuous caster mold[J]. ISIJ International, 1994, 34(3): 255-264.

[41]   Xiaopeng Song, Susen Cheng, Zijian Cheng. Numerical computation for metallurgical behavior of primary inclusion in compact strip production mold[J]. ISIJ International, 2012, 52(10): 1824-1831.

[42]   E. Loth. Numerical approaches for motion of dispersed particles, droplets and bubbles[J]. Progress in Energy and Combustion Science, 2000, 26(3): 161-223.

[43]   Lifeng Zhang. State of the art in the control of inclusions in tire cord steels - A review[J]. Steel Research International, 2006, 77(3): 158-169.

[44]   C. Pfeiler, M. Wu, A. Ludwig. Influence of argon gas bubbles and non-metallic inclusions on the

flow behavior in steel continuous casting[J]. Materials Science and Engineering A, 2005, 413-414(115-120.

[45]   J. U. Brackbill, D. B. Kothe, C. Zemach. A continuum method for modeling surface tension[J]. Journal of Computational Physics, 1992, 100(335-354.

[46]   Petar Liovic, Jong-Leng Liow, Murray Rudman. A volume of fluid (VOF) method for the simulation of metallurgical flows[J]. ISIJ International, 2001, 41(3): 225-233.

[47]   ANSYS FLUENT 14.0[M]. Canonsburg, PA: ANSYS, Inc, 2011.

[48]   Yuji Miki, Brian G. Thomas. Modeling of inclusion removal in a tundish[J]. Metallurgical and Materials Transactions B, 1999, 30(4): 639-654.

[49]   P. G. Mukunda, Shailesh Rao A, Shrikantha S. Rao. Influence of rotational speed of centrifugal casting process on appearance, microstructure, and sliding wear behaviour of Al-2Si cast alloy[J]. Metals and Materials international, 2010, 16(1): 137-143.

[50]   Jan Bohacekn, Abdellah Kharicha, Andreas Ludwig, Menghuai Wu. Simulation of horizontal centrifugal casting: mold filling and solidification[J]. ISIJ International, 2014, 54(2): 266-274.